FACULDADE DE CIÊNCIAS DA UNIVERSIDADE DE LISBOA

Bachelor+Master Degree in Biomedical Engineering and Biophysics

3rd year

INTERNSHIP

Detecting lack of balance during tripping by analyzing signals from IMUs

Teresa Margarida de Campos Pereira

No. 49940

Host institution: The BioRobotics Institute, Scuola Superiore Sant'Anna, Pisa, Italy

Supervisor: Vito Monaco

2019

Acknowledgements

First of all, I would like to thank my supervisor Vito Monaco of The Biorobotics Institute at Scuola Superiore Sant'Anna, for encouraging me to work harder and better, providing me all the support I needed.

I would also like to acknowledge Hugo Ferreira, PhD of the Faculty of Sciences at University of Lisbon, who helped me before the mobility.

For the kindness received and for the financial support, I would like to thank the Student Mobility and Support Area (FCUL) – Ana Paula Matos – and the program Erasmus + from the University of Lisbon – Carlos Pereira.

I would also like to thank my family for giving me the opportunity to experience this internship. I am forever grateful for the unconditional love, for the affection, for all the quick phone calls every day, just to cheer me up. None of this could have happened without you.

I can not forget to thank all my friends for the absolute encouragement and support they gave me. To my scouts' friends, who believe in me more than I do, thank you for all these years full of love, complicity, honesty, adventures and unconditional friendship. You will be forever in my heart.

About my friends Marta Félix and Sara Ponte, I want to affirm that they are the best roommates ever. We spend two months working together and living together, and we never got tired of each other. Thank you for all the movie nights, all the trips in Italy, all the hours spent on doing this report and for making me laugh every day.

I also must thank Mariana Pereira, Tânia Baptista and Luis from Pisa, for our memorable lunches, evenings and ice creams and Mariana Almeida, Cláudia Baleia and Beatriz Neves for the weekend trips as well. I am carrying many memories I will never forget.

Finally, I must thank my boyfriend Gil Nunes, who supported me more than anyone for this last three years, even if we live 255 kilometers away from each other. Let's make this last.

Thank you all!

Abstract

This study aimed to investigate the performance of a pre-impact detection algorithm parsing out the output of a set of Inertial Measurement Units (IMUs) placed on lower limbs and designed to recognize signs of lack of balance due to tripping.

Some young subjects were asked to manage tripping events while walking on a treadmill. An adaptive threshold-based algorithm, relying on a pool of adaptive oscillators, was tuned to identify abrupt kinematics modifications during tripping. Inputs of the algorithm were the acceleration of lower limb segments, as estimated by IMUs located on thighs, shanks and feet.

The results showed that the proposed algorithm can identify a lack of balance in about 0.736 s after the onset of the perturbation, with a 23.80 percentage of false alarms, by combining data related to the perturbed limb (right thigh, shank and foot).

The algorithm can hence be considered a multi-purpose tool to identify different perturbations (i.e., slippage and tripping). In this respect, it can be implemented for different wearable applications (e.g., prosthesis or wearable robots) and adopted during daily life activities to enable on-demand injury prevention systems prior to fall impacts.

Index

List of Figures

List of Tables

1. Introduction

Falling is widely recognized as one of the most important causes of disability in fragile individuals [1]. Several reports agree with the evidence that about 30% of older adults (+65 years of age) fall at least once per year and the percentage increases with ageing and related neuro-muscular-skeletal diseases [22]. Falls can indeed result in traumatic and physiological consequences, thus worsening the quality of life of fragile individuals and augmenting the costs of healthcare.

The increasing life expectancy of the worldwide population is expected to further exacerbate the effects of the risk of falls on society. As such, national and international agencies have been facing this problem by consistently supporting research activities in the field of fall prevention programs.

One of the strategies currently being investigated to counteract the risk of falls involves predicting the forthcoming occurrence using wearable sensors in conjunction with suitable signal processing algorithms [14-17]. Inertial sensors, also named inertial measurement units (IMUs; i.e., accelerometers and/or gyroscopes), are among the most applicable sensor types since they can work as stand-alone platforms during daily activities in unstructured environments and can be easily embedded in wearable devices [5, 14].

Several authors have developed and tested different fall-risk assessment tools, such as machine learning approaches to classify fall risk (e.g., high vs. low) based on the analysis of signals recorded by IMUs during specific assessment tasks (e.g., walking, time up-and-go, sit-to-stand transitions). This approach is frequently used in clinical settings since it allows the stratification of potential fallers in terms of prospective fall risk probability. Nonetheless, they do not distinguish people based on their attitude to manage hazards met during daily activities (e.g., slippery surfaces, carpets). Accordingly, this approach cannot be used to predict a loss of balance that suddenly escalates to a fall. Additionally, others have investigated the effectiveness of a closed-loop strategy combining predictive algorithms that are able to detect signs of incipient falls—the pre-impact fall detection algorithm—with wearable devices designed to counteract the lack of balance. In particular, once the lack of balance is detected, the algorithm employs a wearable device designed to either mitigate the impact with the ground or supply suitable assistance, thus preventing potential injuries.

The aim of this study was to develop and test a novel pre-impact algorithm to detect the lack of balance due to unexpected tripping delivered while steadily walking in well-controlled experimental conditions [18]. This algorithm is based on the evidence that a sudden perturbation (i.e., tripping) alters the quasi-periodic features of steady walking, this highlighting an abnormal behavior that can reflect a lack of balance and, in turn, an incipient fall. In this case, the acceleration of lower limb segments was estimated by processing the data concerning the trajectories of some body markers and then used as input for our pre-impact detection algorithm (PIDA), which was tuned to minimize both detection time and false alarms (FA). After being suitably retuned, it is expected to be able to detect unexpected perturbations by analyzing different types of signals as long as they reflect the rhythmic features of steady walking.

Our PIDA is designed to be implemented in wearable devices (e.g. prosthesis for amputees and wearable exoskeletons for older adults or people with motor disabilities) in order to promote balance recovery when a fall is detected.

2. Concepts

2.1 Human Gait

Kinematic variables are involved in the description of the movement, independent of forces that cause that movement. Kinematics can include linear and angular displacements, velocities and accelerations of body segments and joints during motion.

The act of walking has two basic requisites for any form of bipedal walking:

1. Periodic movement of each foot from one position of support to the next;
2. Sufficient ground reaction forces, applied through the feet, to support the body.

2.1.1 Gait Cycle

There are two main phases in the gait cycle. During *stance* phase, representing around 60% of the cycle, the foot is on the ground, whereas in *swing* phase, representing the other 40%, that same foot is no longer in contact with the ground and the leg is swinging through, in preparation for the next foot strike [19, 21].

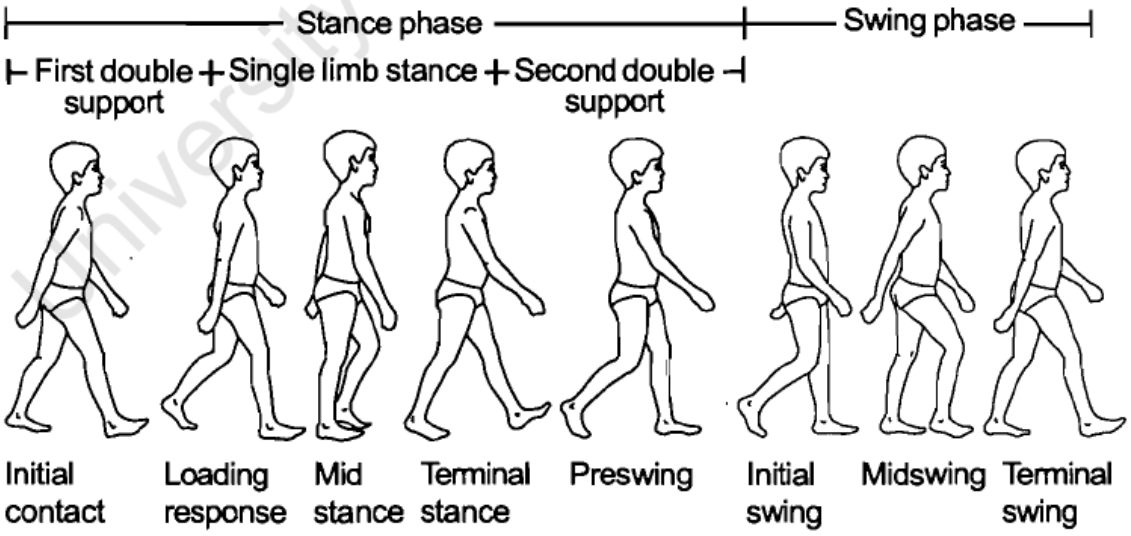

Figure 1: Representation of the Phases and Events of the Human Gait Cycle

As shown in Figure 1**Erro! A origem da referência não foi encontrada.**, both the stance and swing phases are constituted by several events. However, the most relevant events are the ones that represent the beginning and the end of the stance phase. The initial contacts is called *Heel Strike* and it represents the beginning of the gate cycle. The pre-swing is usually called *Toe-off* and it is, as the name indicates, the moment the foot leaves the ground and, consequently the beginning of the swing phase.

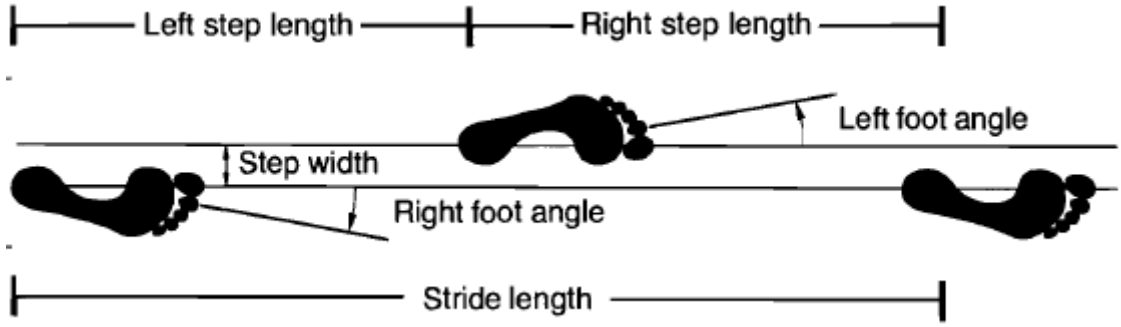

Figure 2: Distance parameters provided by a person's footprints

Whereas Figure 1 emphasizes the temporal aspects of human gait, Figure 2 illustrates how a set of footprints can provide useful distance parameters. *Stride Length* is the distance travelled by a person during one stride (or cycle) and it can be measured as the length between the heels from one heel strike to the next heel strike of the same foot. Two step lengths (left plus right) make one stride length.

Measuring all these components of the gait cycle allows to calculate some kinematical parameters related to someone's movement.

2.2 Rigid Bodies and Reference Frames

A rigid body is considered as a continuous distribution of mass, in which the distance between any two given points on it remain constant in time, regardless of external forces exerted on it.

The position of a rigid body is the position of all the particles of which it is composed, even though it is possible to describe the position of at least three non-collinear particles. This makes it possible to reconstruct the position of all the other particles, provided that their time-invariant position relative to the three selected particles is known.

2.2.1 Human Body Landmarks

A human anatomical landmark is a point in the human body which remains preserved between and within the different human body shapes, and it must be visible at the surface. Anatomical landmarks can be, for example, center of gravity of body segments, centers of rotation of joints, extremes of limb segments, or key anatomical prominences.

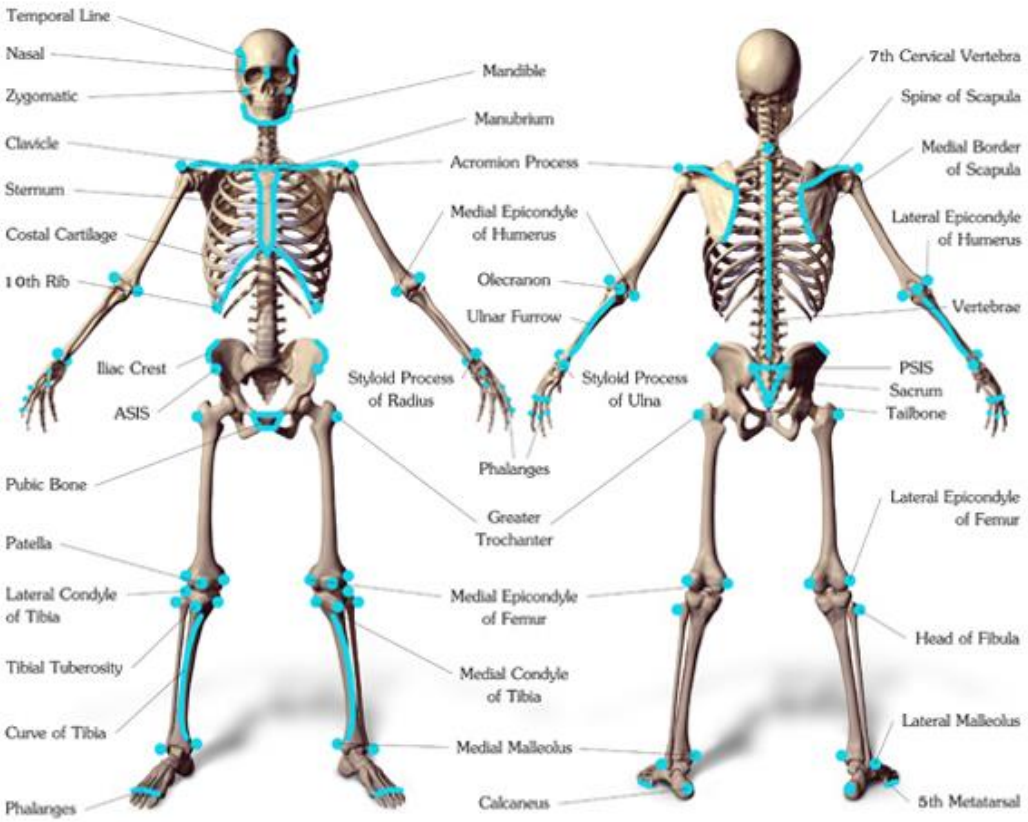

Figure 3: Example of some possible anatomical landmarks of the Human Body

2.2.2 Reference System

In order to keep track of all the kinematic variables, it is important to establish a conventional system which allow us to describe a movement using terms as *proximal, flexion* and *anterior.*

The spatial reference system can be either relative or absolute. The first one requires all coordinates to be relative to an anatomical coordinate system that changes from segment to segment. An absolute system means that the coordinates are referred to an external spatial reference system.

In Biomechanics, the most used reference system is orientated as follows:

1. X-axis: Represents the direction of progression (anterior-posterior);
2. Y-axis: Represents the vertical direction;
3. Z-axis: Represents the sideways direction (medial-lateral); [21]

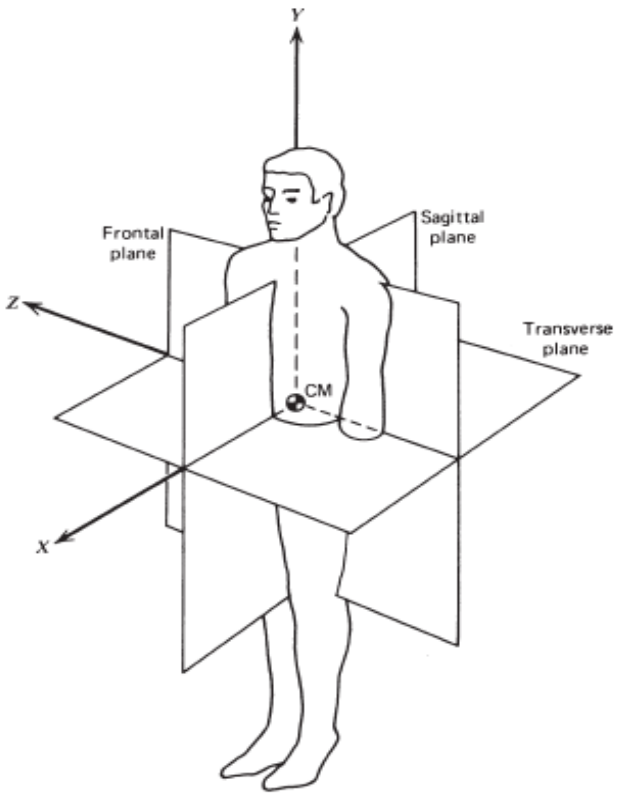

Figure 4: Reference System according to International Society of Biomechanics (ISB) recommendations

2.2.3 Human Anatomical Frames

The anatomical frames are relative reference systems, as mentioned above, and allow an easy interpretation of the movement. To define a reference frame in some body segment, taking a body landmark as the origin, *Reynolds* has made the following recommendations:

- The coordinate directions must comply with the right-handed rule;
- An axis system must be defined using three non-collinear anatomical landmarks that are on a rigid body; [14]

2.3 IMUs

An IMU, inertial measurement units, is a self-contained system that measures linear and angular motion of an object in free space relative to an inertial frame. Sensors for inertial measurement consist primarily of a 3-axis accelerometer and a 3-axis gyroscope, which would be considered a 6-axis IMU.

This type of systems provides two to six DOF (Degrees of Freedom), which refers to number of different ways that an object is able to move throughout 3D space. The maximum possible is 6 DOF, which would include three degrees of translation movement across a straight plane or along each axis (front/back, right/left, up/down) and three degrees of rotational movement across the x, y, z axes.

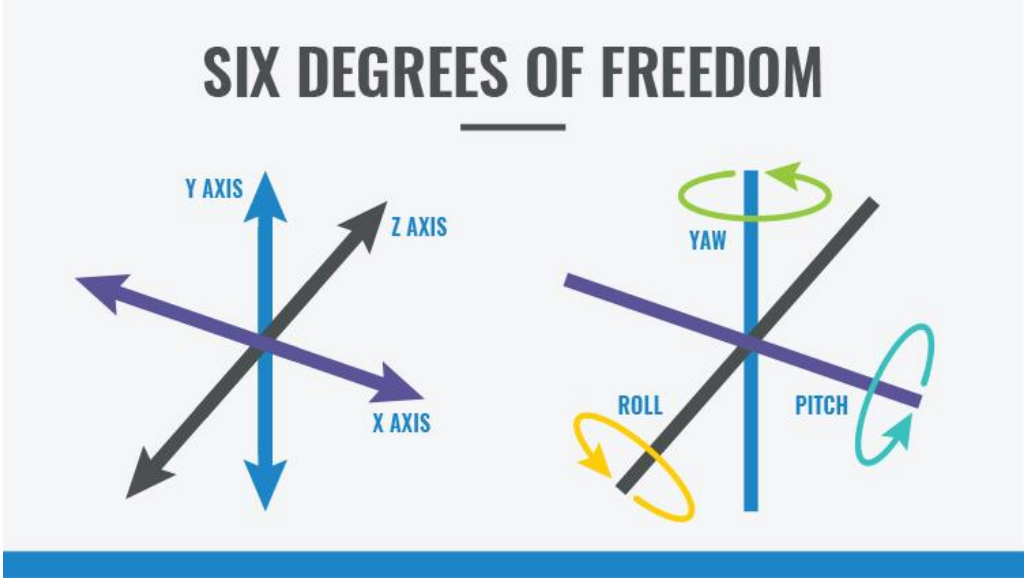

Figure 5: Representation of the six degrees of freedom.

2.3.1 Accelerometer

The most commonly used type of motion sensor is the accelerometer. There are simple and triaxial accelerometers, which measure linear acceleration across a single axis and across the three axes, respectively.

2.3.2 Gyroscopes

Gyroscopes measure angular velocity about thee axes: pitch (x axis), roll (y axis) and yaw (z axis). When integrated with sensor fusion software, a gyro can be used to determine an object's orientation within 3D space.

3. Materials and Methodology

3.1 Experimental Protocol

Some young subjects between 18 and 30 years old, were asked to walk at their self-selected speed, on a treadmill. While they were walking, they were exposed to unexpected tripping-like perturbations delivered to the right leg during its swing phase. For safety reasons, the treadmill was provided with handrails allowing participants to grasp them only in case of unrecoverable lack of balance. Otherwise, they were not allowed to use the handrails during the entire experimental session [1].

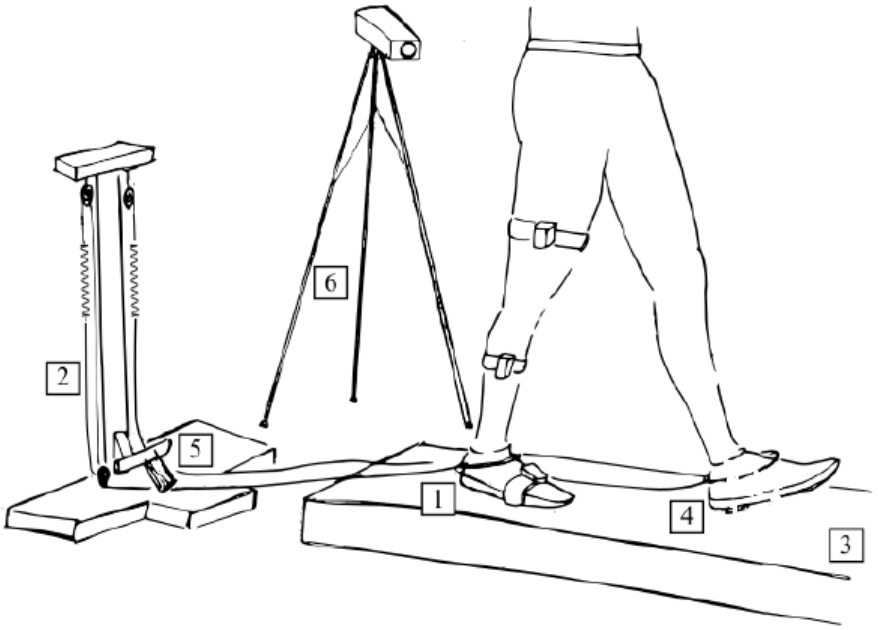

Figure 6: Schematic of the experimental setup. Labeled components are: 1. Perturbed foot; 2. Spring-rope mechanism; 3. Treadmill; 4. Footswitch under the unperturbed foot; 5. Cam-based braking mechanism; 6. Camera-based motion system.

During each experimental session, 3D kinematics of a set of 25 reflective spherical was recorded with a sample rate of 100 Hz, by using an eight camera-based system. In particular, the markers were divided in order represent different lower limbs segments (i.e., pelvis, thighs, shanks and feet).

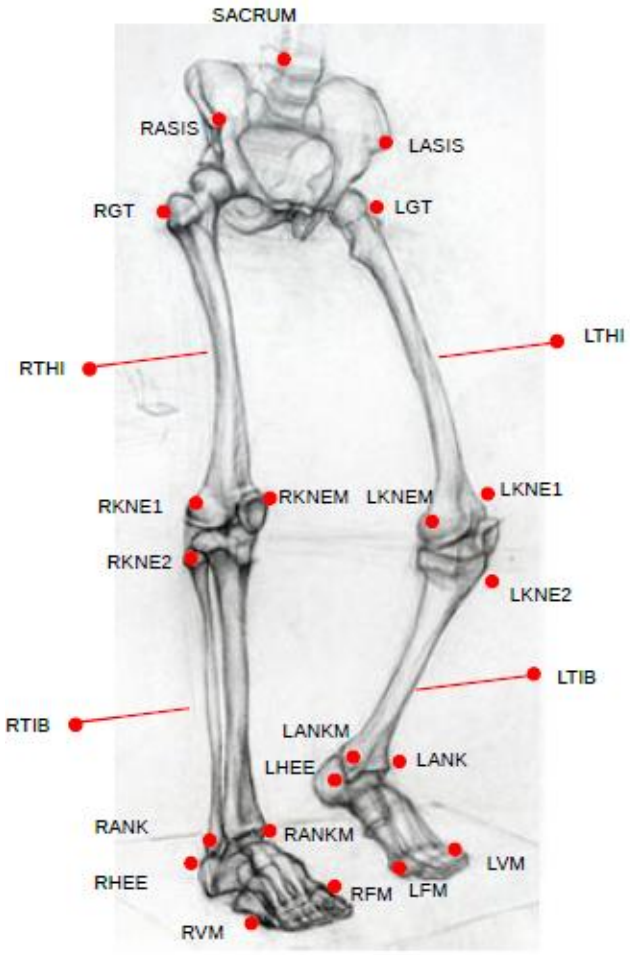

Figure 7: Set of 25 markers used on this study.

The global reference frame was located in the center of the treadmill and its axes were oriented as follows: y-axis was oriented in the opposite direction of progression; the z-axis was vertical toward upward; the x-axis was medio-lateral, in accordance with the right-hand-rule.

3.2 Data Processing

The 3D trajectory of each marker was exported and represented our raw data. Since the raw data had some missing information due to some positions that the camera-system could not reach, interpolation was computed in order to fill the empty samples with estimated data.

Firstly, high-frequencies related to noise and artifacts were removed by applying a 4^{th} order low-pass Butterworth filter, with cut off at 10 Hz. After that, the global reference frame mentioned in section 3.1 was changed to a new one based on the ISB (International Society of Biomechanics) reference system, presented in Figure 4.

Having all the raw data concerning the trajectories of the markers projected in the new reference system, gate events (i.e., right and left heel strikes) were identified by computing the maximums of the x component of the heel markers (RHEE and LHEE). Since the tripping events were delivered after some of the right HS, the onset of the perturbations could be estimated by finding the samples corresponding to a lower heel strike, as presented in Appendix B.

The first step to calculate the acceleration of each body segment was to find a local reference frame to all the segments, except pelvis (i.e. right and left feet, right and left shanks, right and left thighs), choosing one of the markers of that segment to represent the origin [

Appendix A]. Then, the acceleration was computed calculating the second derivative of the positions. Finally, knowing the acceleration of each body segment, the last step was to project that acceleration in the local reference frame, using rotational matrices.

The plots of the acceleration of each body segment were created and they represented the variation of the acceleration ($m.s^{-2}$) in terms of time (s).

Once
Furthermore,

3.3 Pre-Impact Detection Algorithm (PIDA)

Our
3.3.1
If

To achieve the optimal tuning of the set of AOs, we firstly investigated the dynamic behavior of the AOs in the domain of the learning gain parameters allowing the best match between measured and estimated acceleration during steady walking. The Root Mean Square Deviation (RMSD) between measured and estimated signals was calculated as

$$RMSD = \sqrt{\frac{\sum_{t=1}^{T}(\hat{y}_t - y_t)^2}{T}}$$ [Equation 1]

In the equation, $\hat{y}_t$ is the estimated signal, y_t is the measured signal and T is the total number of samples.

In general, a low RMSD means that the estimated signals are similar to the measured one. Consequently, the optimal parameters are achieved when RMSD is as low as possible.

The difference between input and output, namely *error*, should be close to zero, if the parameters K_A and K_P are suitable. This error is then analyzed by a threshold-based algorithm.

3.3.2 Threshold-Based Algorithm

Once the AOs were properly set up, we tuned the adaptive threshold-based algorithm in order to both minimize the detection time and reduce the percentage of false alarms.

The inputs to this algorithm were:

a. Signal, which is the error mentioned in section 3.3.1 Adaptive Oscillator;
b. R, which represents the number of warnings;
c. K, which represents the amplitude of the threshold, in terms of standard deviation.
d. Q, which represents the maximum samples that can occur between R consecutive warnings to be considered a lack of balance.
e. P, which represents the time (in terms of samples) the AOs requires to return an estimated signal similar to the actual;

The output were:

a. **Detection Time (DT):** the time elapsed between the onset of the perturbations and the output of the algorithm;
b. **False Negative (FN):** a false alarm occurring when no lack of balance was detected within 1 second (100 samples) after the onset of the perturbation;
c. **False Positive (FP):** a false alarm occurring when a lack of balance was detected before the actual perturbation [21].

Therefore, the algorithm was implemented as follows:

1. The mean (μ) and standard deviation (σ) of the input signal are computed.
2. A threshold is set at $-\mu - \sigma K$, where K is a factor to shape the value of threshold, as mentioned above.
3. The minimums of the error are computed, and a warning is recorded when one minimum is above the threshold. It is essential to eliminate the warnings occurring during the first P samples, due to the error not being stabilized yet.
4. When R consecutive warnings were recorded in less than Q samples, the algorithm detects a lack of balance.

The performance of our PIDA was assessed in terms of mean detection time (MDT) and percentage of FA across subjects.

4 Results

4.1 Computing the Acceleration

Once tripping occurs when a foot, unexpectedly, in its swing phase, collides an object causing a lack of balance, the perturbations are easily identified on the acceleration of the foot. Thus, the accelerations of shanks and thighs for each subject are presented in Appendix C.

To have a better view of the perturbations, a region of interest around the onset of one perturbation was chosen. The following figures are the representation of the different signals in that region.

4.1.1 Subject 1

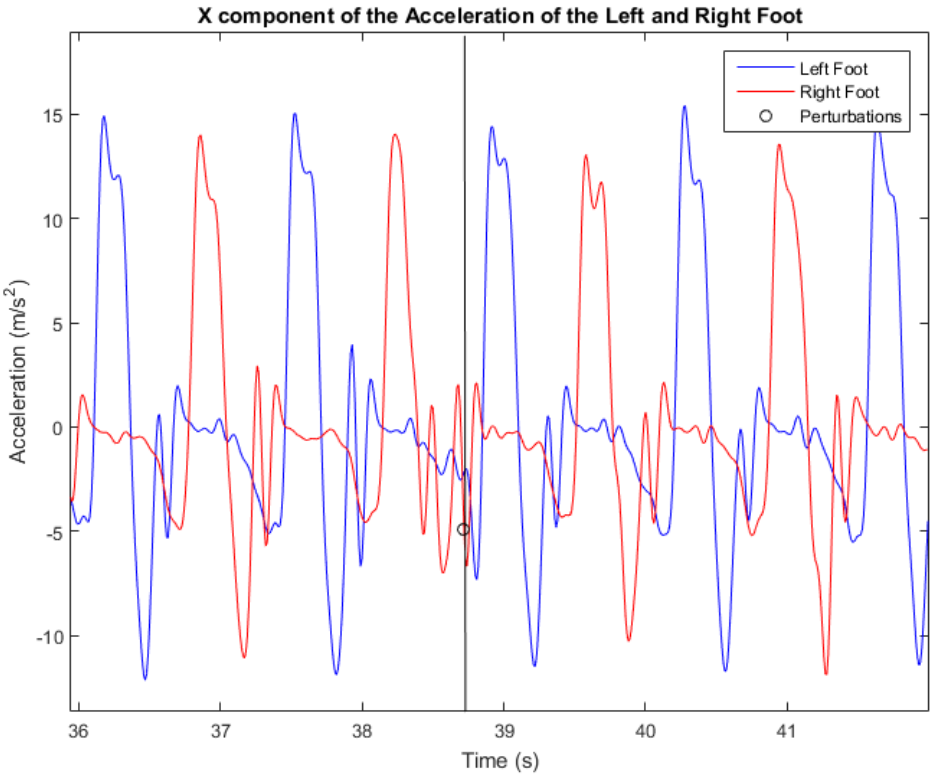

Figure 8: A region of interest of the X component of the acceleration ($m.s^{-2}$) of both left (blue) and right (red) feet, in terms of time (s), for subject 1. The perturbation is presented in black.

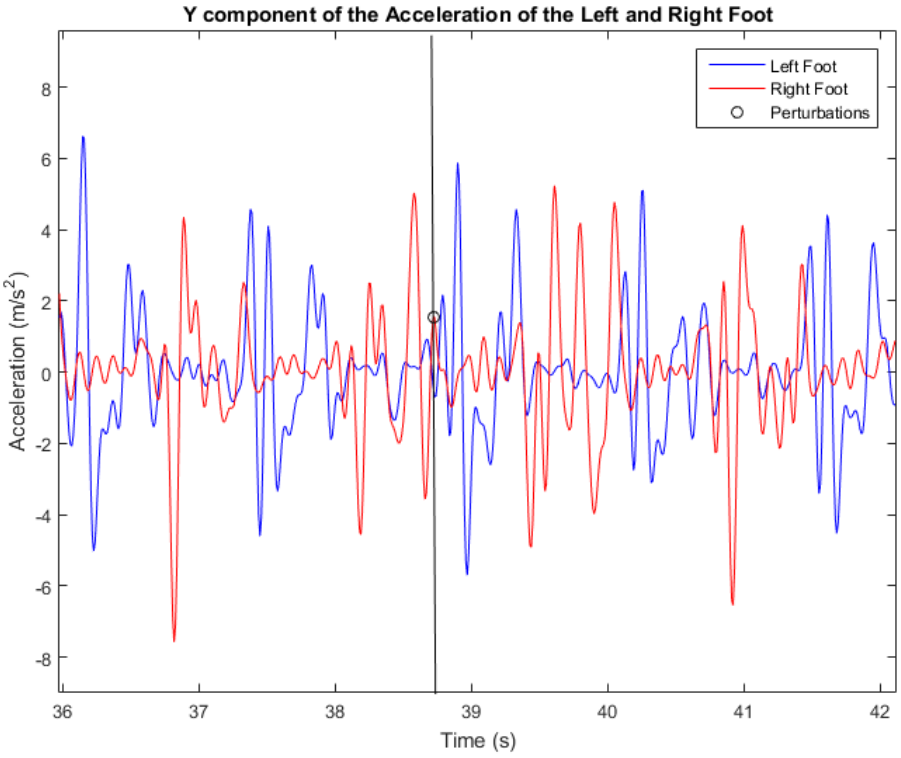

Figure 9: A region of interest of the Y component of the acceleration ($m.s^{-2}$) of both left (blue) and right (red) feet, in terms of time (s), for subject 1. The perturbation is presented in black.

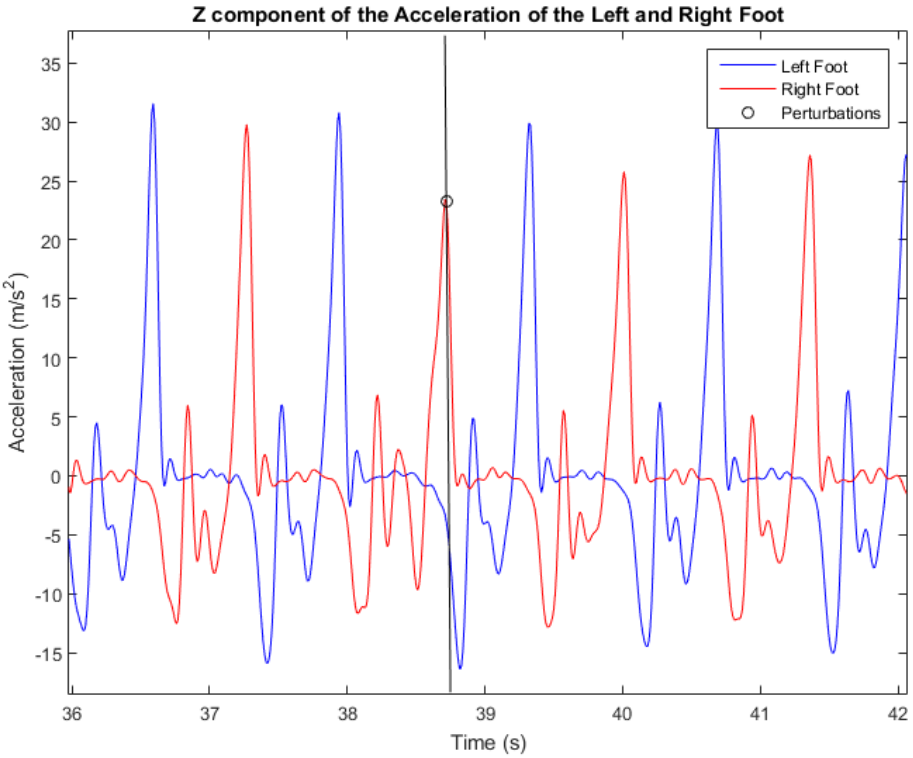

Figure 10: A region of interest of the Z component of the acceleration ($m.s^{-2}$) of both left (blue) and right (red) feet, in terms of time (s), for subject 1. The perturbation is presented in black.

4.1.2 Subject 2

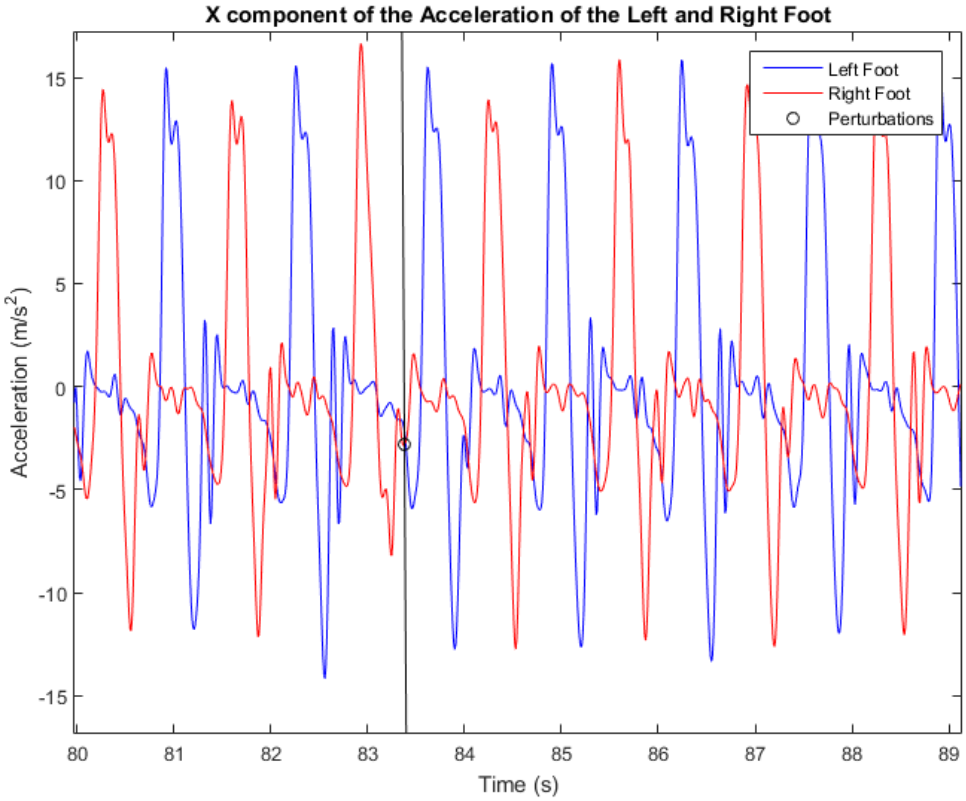

Figure 11: A region of interest of the X component of the acceleration ($m.s^{-2}$) of both left (blue) and right (red) feet, in terms of time (s), for subject 2. The perturbation is presented in black.

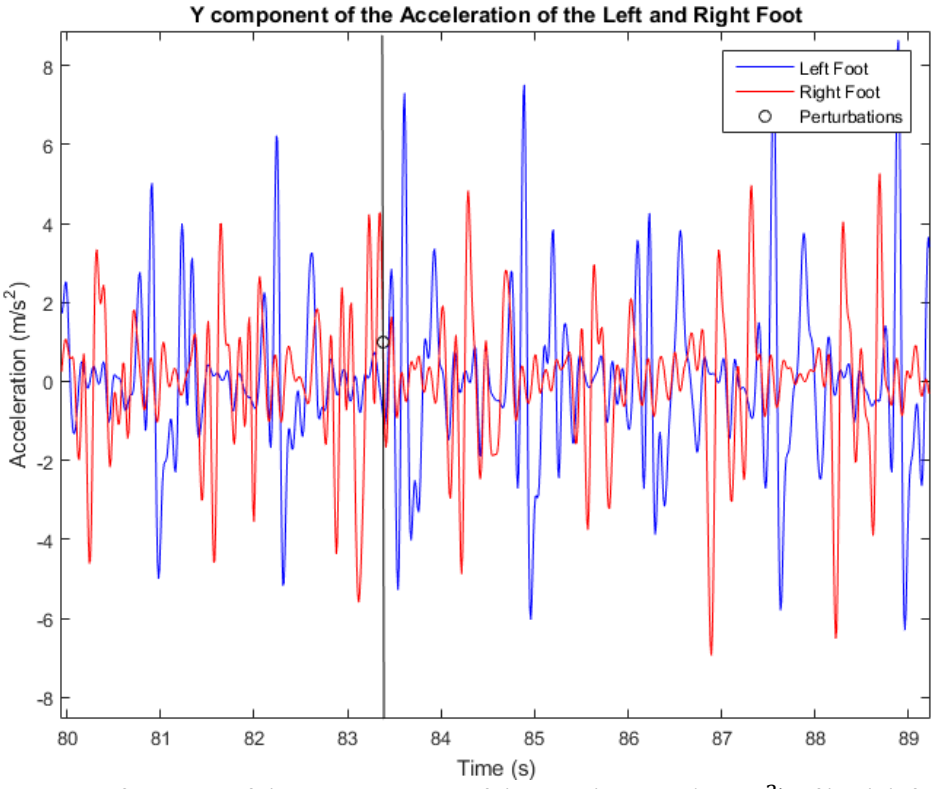

Figure 12: A region of interest of the Y component of the acceleration ($m.s^{-2}$) of both left (blue) and right (red) feet, in terms of time (s), for subject 2. The perturbation is presented in black.

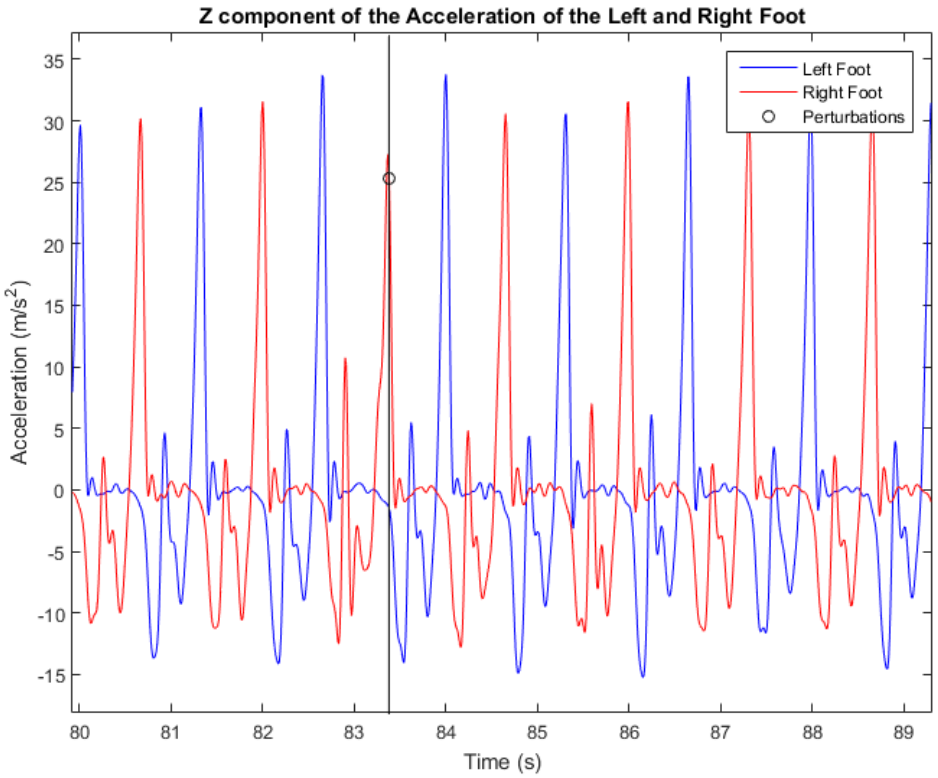

Figure 13: A region of interest of the Z component of the acceleration ($m.s^{-2}$) of both left (blue) and right (red) feet, in terms of time (s), for subject 2. The perturbation is presented in black.

4.2 Tuning the Parameters for the AOs

As mentioned in the methodology, the PCA was applied to the acceleration signals, in order to combine all the information and achieve a new signal that still contains the most relevant information of each acceleration, which means that the perturbations are still easily identified.

The best signal was achieved when the PCA was applied to the three components of the acceleration of each body segment of the right lower limb. We can find some other combinations tested in **[APPENDIX D].**

The PCA signal is the input to the Adaptive Oscillators and the error represents the difference between the real and the estimated signal.

4.2.1 Subject 1

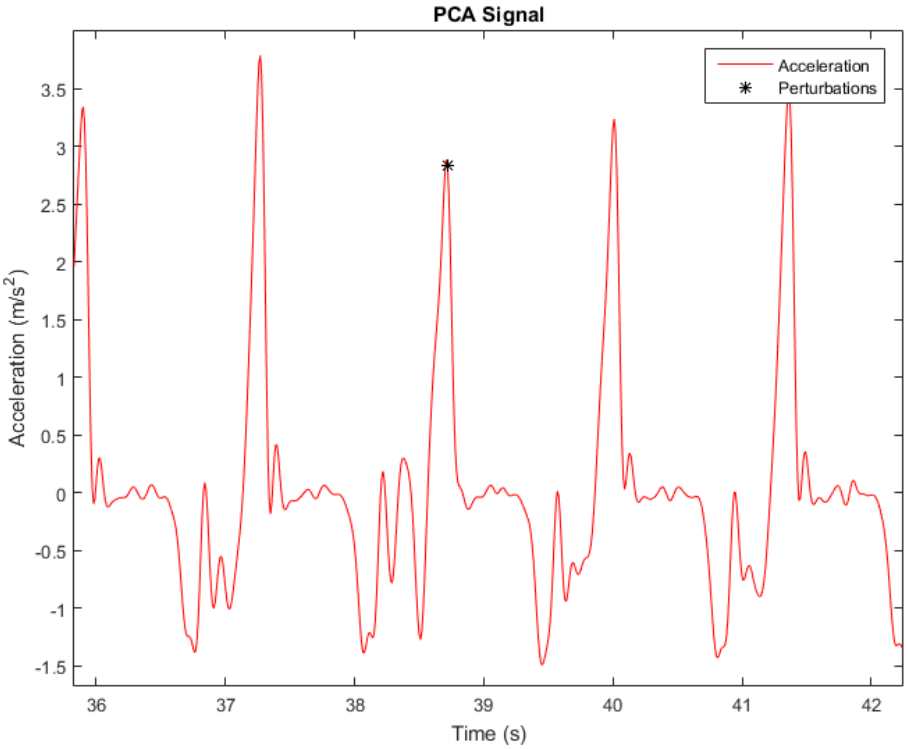

Figure 14: A region of interest of the signal obtained by applying the PCA to the three components of the acceleration of the right foot, shank and thigh, for subject 1. The perturbation is presented in black.

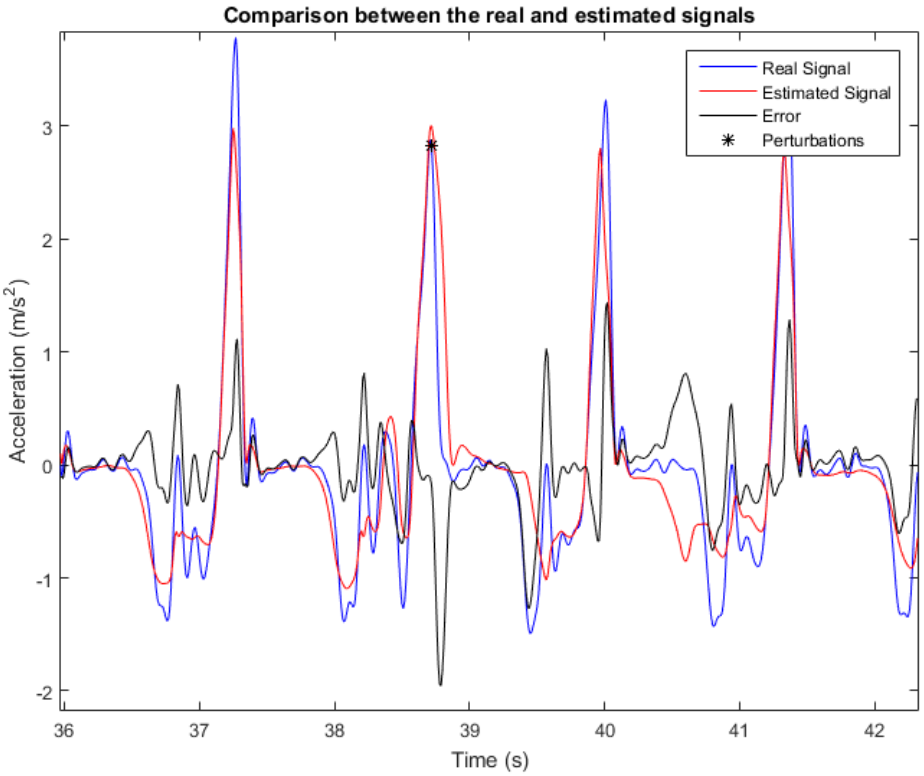

Figure 15: Comparison between the real signal (blue) and the estimated signal (red). The learning gains, K_A and K_P, are 5 and 0.1, respectively, for subject 1. The error is represented in black.

4.2.2 Subject 2

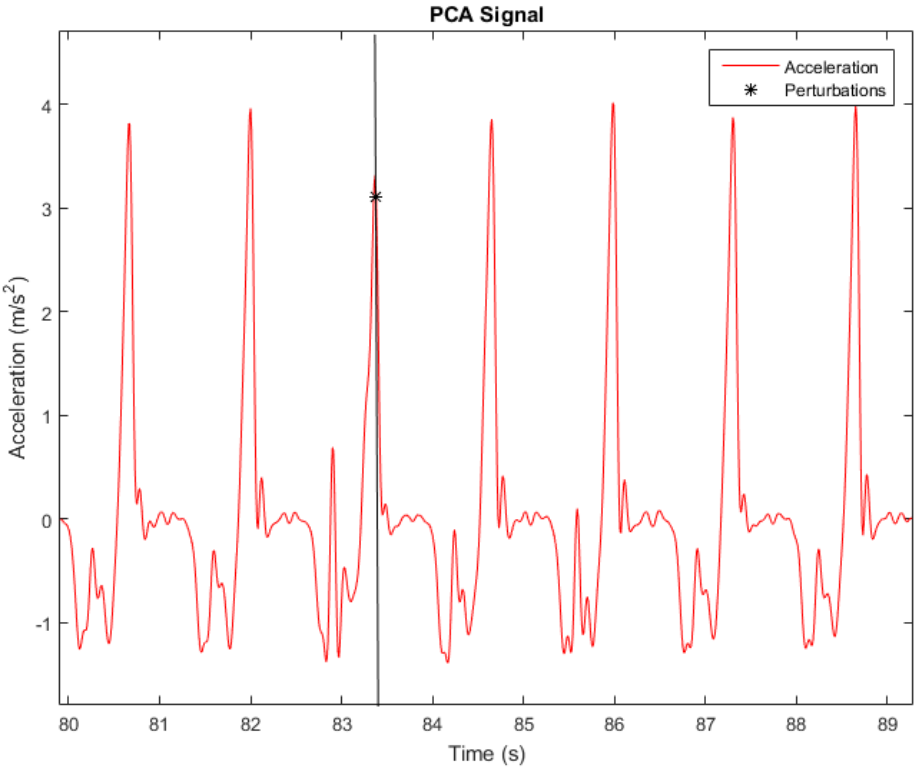

Figure 16: A region of interest of the signal obtained by applying the PCA to the three components of the acceleration of the right foot, shank and thigh, for subject 2. The perturbation is presented in black.

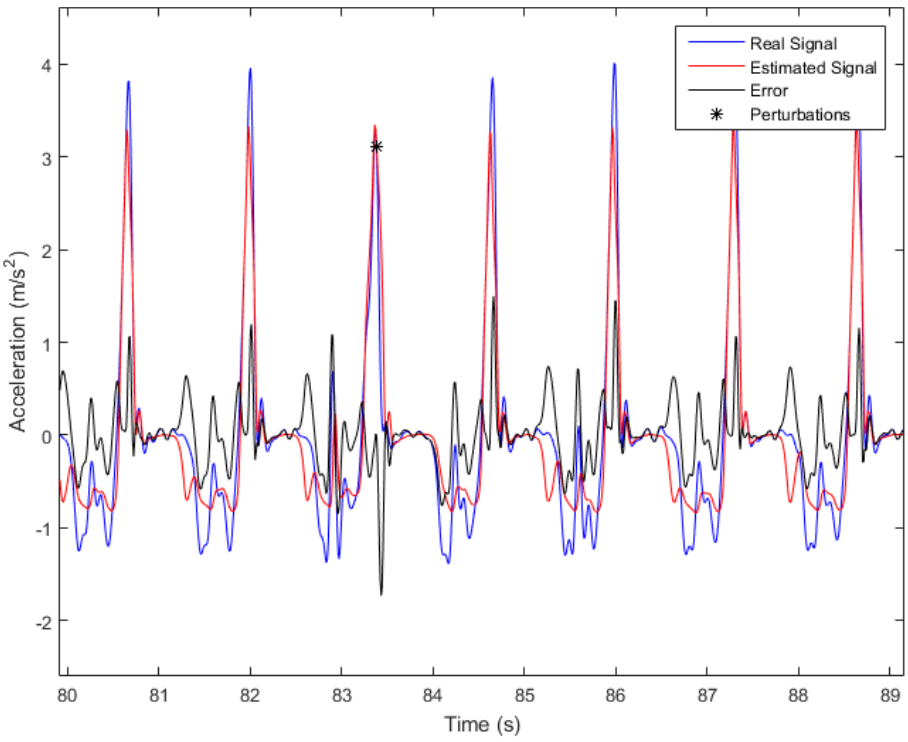

Figure 17: Comparison between the real signal (blue) and the estimated signal (red). The learning gains, K_A and K_P, are 1 and 0.1, respectively, for subject 2. The error is represented in black.

4.3 Threshold-based algorithm results

The Threshold-based algorithm detects lack of balance and evaluate whether the detected point is a false alarm or an actual tripping detection.

The following sub-sections show the outputs of the algorithm, such as the detected points presented in the figures and the Mean Detection Time and Percentage of False Alarms in the table.

4.3.1 Subject 1

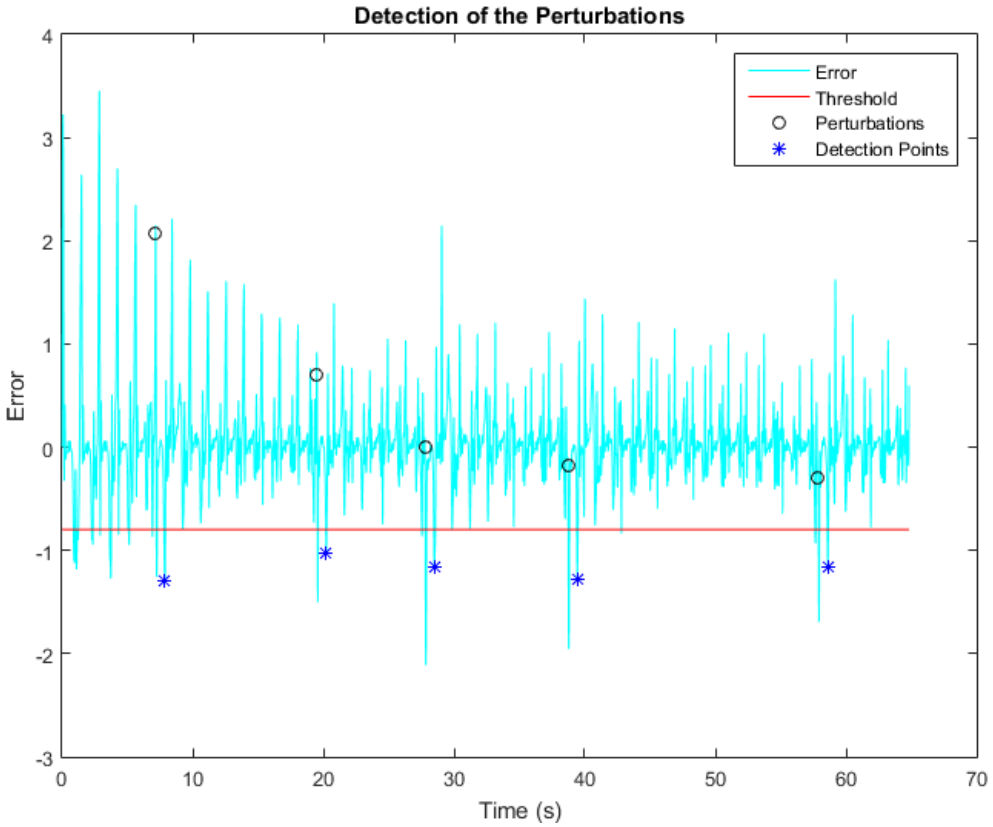

Figure 18: Representation of the detection points provided by the threshold algorithm, for subject 1. The blue signal is the error; the red horizontal line is the threshold; the black points represent the perturbations and the blue stars represent the detection points.

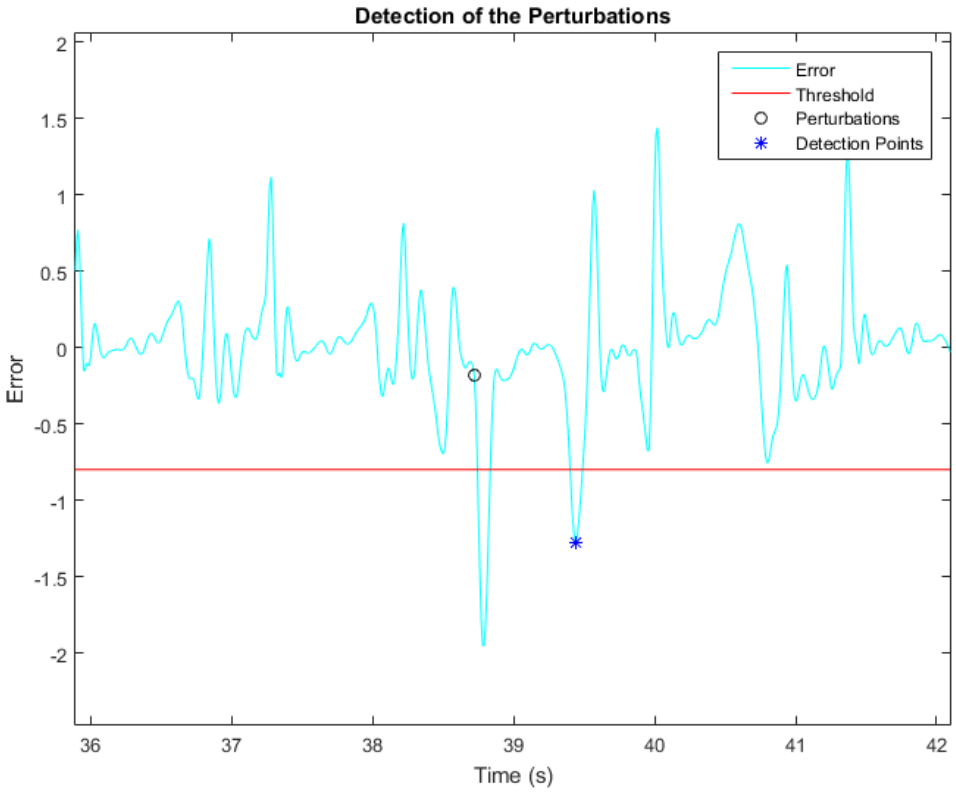

Figure 19: Representation of the detection point in the region of interest chosen, for subject 1.

4.3.2 Subject 2

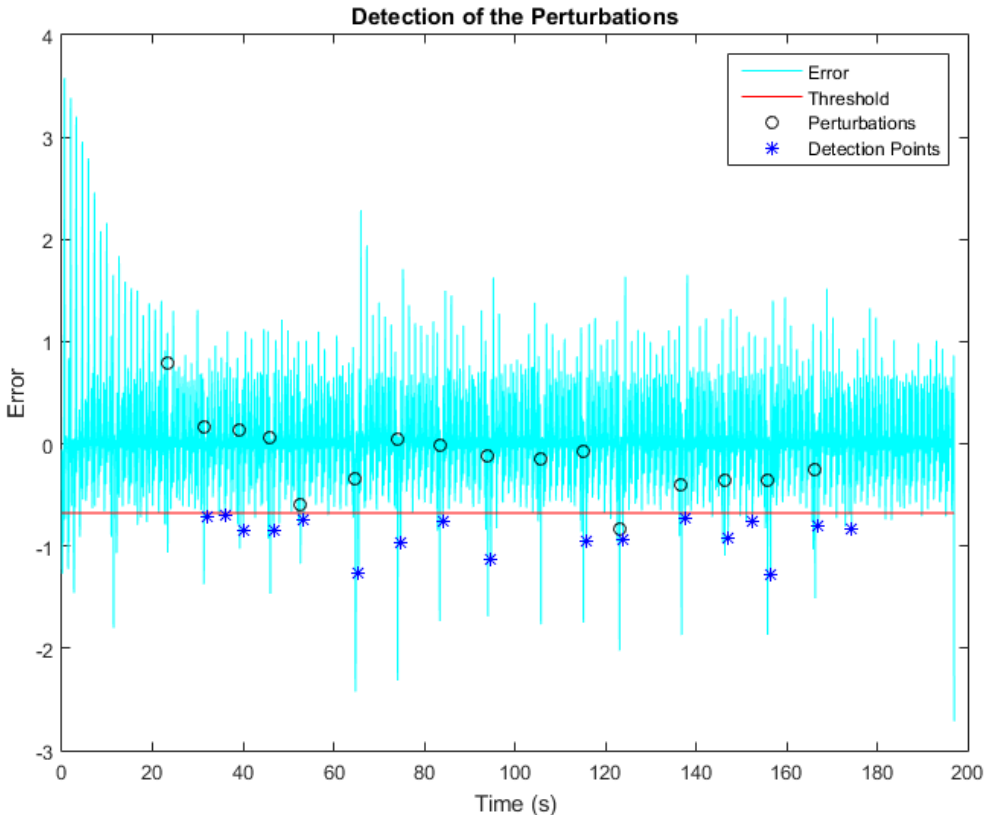

Figure 20: Representation of the detection points provided by the threshold algorithm, for subject 2. The blue signal is the error; the red horizontal line is the threshold; the black points represent the perturbations and the blue stars represent the detection points.

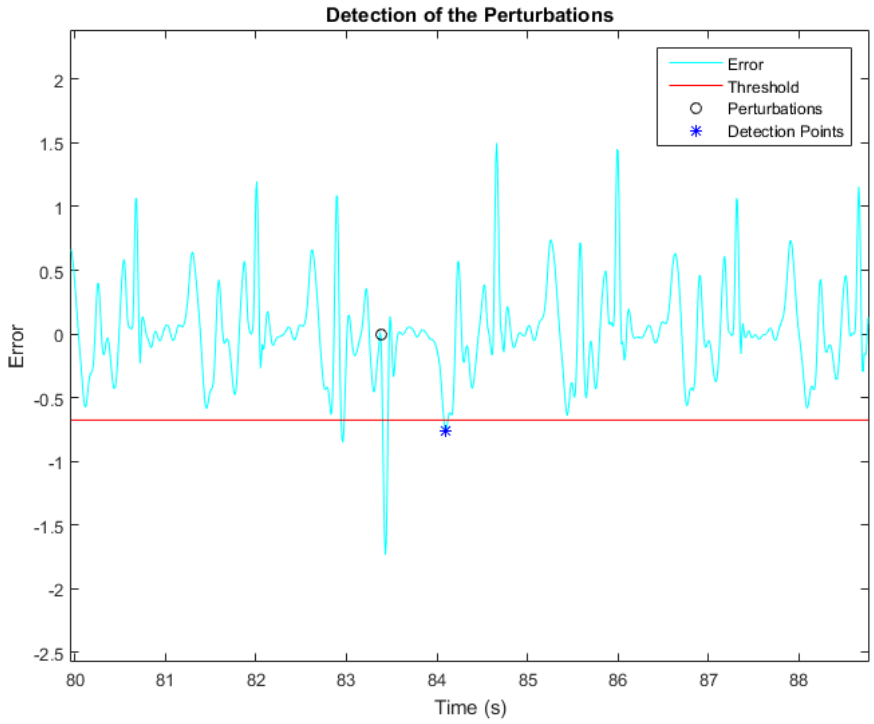

Figure 21: Representation of the detection point in the region of interest chosen, for subject 2.

To evaluate the performance of the algorithm, we calculated the mean detection time, as well as the percentage of False Alarms, across both subject and we achieved the following results:

Table 1: Performance of the Threshold-Based Algorithm across both subjects.

MEAN DETECTION TIME (ms)	NUMBER OF FALSE NEGATIVE ALARMS	NUMBER OF FALSE POSITIVE ALARMS	PERCENTAGE OF FALSE ALARMS
736.45	2	3	23.80%

5 Discussion

The aim of this study was to develop a suitable algorithm parsing IMUs signals data to detect lack of balance due to unexpected tripping in less than one second and with a rate of false alarms lower than 10%, in order to be implemented in a wearable device that promote balance recovery.

The data processing was particularly important to create the reference frames in each body segment, which allowed us to estimate an accelerometer signal in each segment by performing the acceleration in the origins.

In Appendix B, it is visible that the perturbations were identified around the samples 3870 and 8370, for subject 1 and subject 2, respectively, since they correspond to a lower Heel Strike of the Right Foot. By analyzing the acceleration of the right foot around these samples, it is noted that it lost its periodicity. In particular, in x and z components we can easily identify a change in its pattern around the samples corresponding to a perturbation, whereas the contribution of the vertical component to identify the tripping events was not so significant, since the signal has many oscillations that do not allow us the identify a pattern and consequently a loss of it. This evidence is valid for shank and thigh as well. Due to the tripping events being exposed only on the right foot, the acceleration of the left foot kept its behavior across all the samples, as expected.

To combine the nine signals concerning the three components of the acceleration of the three right segments (foot, shank and thigh), we applied the principal component analysis, which compressed those signals to only one in which the perturbations are still visible, as we can verify in Figure 1414 and Figure 1666.

Regarding the pool of Adaptive Oscillators, to achieve its optimal tuning, we had to investigate the dynamic behavior of the AOs in the domain of learning parameters allowing the best match between measured and estimated acceleration during steady walking, by finding the lowest value of RMSD.

Noticing that the PCA signals oscillates a lot, we could not find parameters which enable the AOs to estimate a signal sufficiently synchronized with the input. As a result, the error is not close to zero during steady walking, as it was supposed to. Nevertheless, the error increases substantially after the perturbations, as shown in Figure 1555 and Figure 1777, so it is still viable to use it as an input for the threshold-based algorithm.

Concerning this last algorithm, it is important to emphasize that the first trials contained many detected points below the threshold because the error was not stabilized yet. Consequently, the first trials (since the first sample until 100 samples before the first perturbation) were eliminated. When it comes to the input parameters of the algorithm, it is possible to infer that:

- If the K is great, fewer points would be detected and, therefore, the algorithm could miss the detection of one perturbation. On the other hand, having a lower K, may result in too much False Alarms detected;
- By having a great value of R, the number of warning increases, which can lead to both a reduction of FA and an increase of the MDT (more warning would be needed to detect a perturbation).

The detection time is calculated by performing the time difference between the black points and the following blue stars. In Figure 17, a false alarm positive is presented around the 152 seconds, where we can find a detection point before the actual perturbation. A false alarm negative is presented around the time 105 seconds, where we find a perturbation that is not detected by the algorithm. Figure 17

Overall, we obtained a total percentage of false alarms of 23.80% and a mean detection time (MDT) of 736.45 ms. Even though the algorithm can detect a lack of balance in its earliest stage, the rate of False Alarms is much above 10%, which is the ideal, as mentioned in literature.

Hence, to have a better performance of our algorithm, we need to find a solution to decrease the rate of false alarms.

Then, we should redefine the parameters K and R, particularly increasing both, in order to decrease the number of false alarms. Besides this redefinition, applying the principal component analysis merely to the x and z components of the acceleration of the three right segments could also be a solution to achieve more effective and efficient results once we eliminate the vertical component that provokes many oscillations in the signal. This could lead to an error signal closer to zero and, consequently, an easier identification of the perturbation which may result in less false alarms.

These results corroborate the hypothesis that the proposed algorithm can timely detect the lack of balance due to tripping delivered during steady walking, even though there are several parameters that need to be better tuned in order to achieve a better performance.

6 Conclusion

In this study, a pre-impact detection algorithm was designed to identify the lack of balance due to tripping. The best performance was obtained when analyzing the acceleration of the right segments with a mean detection time equal to 736.45 ms and a rate of false alarms of 23.80%, greater than expected, which means that some readjustments are requested in order to decrease this percentage. After that, it can be easily implemented in a lower limb robotic prosthesis or in a wearable exoskeleton (for amputees and older, respectively) already equipped with sensors to provide assistance to the user, while regaining balance after unexpected tripping.

Although promising, the performances of our detection algorithm are limited by the fact that it was tested and validated under well-controlled experimental conditions. In this respect, the cyclic features of the unperturbed gait patterns were guaranteed by a constant walking speed, in contrast to the evidence that human behavior, in real life, is much more variable (e.g., walking speed changes continuously, while walking people can change direction, or climb/descend stairs). In addition, the lack of balance was induced by pseudo-impulsive events (i.e., unexpected tripping), whereas a real fall is a complex motor task involving no-stereotyped biomechanics. In addition, the algorithm was tested only to healthy and young subjects, which is also a limitation of it.

Finally, we used the simplest approach (i.e., a threshold-based algorithm parsing only one signal) to detect abnormal behaviors even if a more complex strategy can be also implemented to improve the overall performance. Accordingly, future analysis will be focused on testing and updating the proposed algorithm to detect real-world falls, as well as evaluate the performance of the algorithm with older people or amputees.

During this internship, I found myself able to work alone and to be autonomous while doing my work. I have done a lot of research about biomechanics by reading papers and searching on the Internet, in order to learn new concepts and be able to achieve good results. In addition, I had the opportunity to meet other cultures, other ways of thinking, other gastronomy, other cities and places. To conclude, this experience allowed me to grew up as a person and student and I am truly proud of myself for being able to be far away from all the people I love for two months.

References

1. Aprigliano, F, M Guaitolini, A.M Sabatini, S Micera, and V. Monaco. *Pre-Impact detection algorithm to identify lack of balance due to tripping-like Perturbations.* Berlin, Germany: In proceedings of the IEEE Internation Conference of Engineering in Medicine and Biology, 23-27 July 2019.

2. Aprigliano, F., S. Micera, and S. Monaco. "Pre-Impact detection algorithm to identify tripping events using wearable sensors." Pisa, Italy, n.d.

3. Bagalà, F., et al. *Evaluation of Accelerometer-Based Fall Detection Algorithm on Real-World Falls.* Antony Bayer, Cardiff University, United Kingdom, 2012.

4. Daffertshofer, A., C.J.C. Lamoth, O.G. Meijer, and P.J. Beek. "PCA in studying coortination and variability: a tutorial." Netherlands, 2004.

5. Delahoz, Y.S., and M.A. Labrador. "Survey on Fall Detection and Fall Prevention Using Wearable and External Sensors." Sensors 2014.

6. Filippeschi, A., N. Schmitz, M. Miezal, G. Bleser, E. Ruffaldi, and D. Stricker. "Survey of Motion Tracking Methods Based on Inertial Sensors: A focus on Upper Limb Human Motion." Pisa, Italy, 2017.

7. Kangas, M.M, I. Winblad, and T. Jamsã. *Determination of simple threshold for accelerometry-based parameters for fall detection.* IEEE Conference of Engineering in Medicine and Biology Society, 2007.

8. Montesinos, L, R Castaldo, and L Pecchia. *Wearable Inertial Sensors for Fall Risk Assessment and Prediction in Older Adults: A Systematic Review and Meta-Analysis.* IEEE Trans. Neural Syst. Rehabil, 2018.

9. Montesinos, L, R Castaldo, and L. Pecchia. *Wearable Inertial Sensores for Fall Risk Assessment and Prediction in Older Adults: A Systematic Revied and Meta-Analysis. .* IEE Trans. Neural Syst. Rehabil, 2018.

10. Orendurff, M.S., J.A. Schoen, G.C. Bernatz, Segal A.D., and G.K. Klute. *How Human Walk: Bout duration, steps per bout and rest duration.* Journal of Rehabilitation Research & Development, 2008.

11. Palmerini, L., F. Bagalà, A. Zanetti, J. Klenk, C. Becker, and A. Cappello. "A Wavelet-Based Approach to Fall Detection." Bologna, Italy, 2015.

12. Park, S.H. "Tools for assessing fall risk in the elderly: A systematic review and meta-analysis. ." 2018.

13. Rajagopalan, R, L Litvan, and Jung I.P. *Fall Prediction and Prevention Systems: Recent Trends, Challenges, and Futute Research Directions.* Sensors, 2017.

14. Reynolds, Herbet M., and Robert P. Hubbard. "Anatomical Frames of Reference and Biomechanics." Department of Biomechanics, Michigan State University, East Lansing, Michigan, n.d.

15. Sabatini, A., C. Martelloni, S. Scapellato, and F. Cavallo. *Asessment of Walking Features from Foot Inertial Sensing.* IEEE Transactions on Biomedical Engineering, 2005.

16. Sun, R.P, and J.J. Ssosnoff. *Novel Sensing Techology in fall risk assessment in older adults: A systematic review.* BMC Geriatr. , 2018.

17. Tropea, P, N Vitiello, D Martelli, F Aprigliano, S Micera, and V. Monaco. *Detecting Slipping-Like Perturbations by Using Adaptive Oscillators.* Ann. Biomed. Eng, 2014.

18. Tsai, Y., T.T. Tu, H. Bae, and P.H. Chou. "EcoIMU: A dual triaxial-accelerometer inertial measurement unit for wearable applications." n.d.

19. Vaughan, Christopher Leonard. "The Biomechanics of Human Locomotion." University of Cape Town, August 2009.

20. WHO. *WHO Global Report on Falls Prevention in Older Age.* Geneva, Switzerland: World Health Organization, 2018.

21. Winter, David A. *Biomechanics and motor control of human movement.* JOHN WILEY & SONS, INC, 2009.

Appendix A

A.1 Origins and Orientation of the local reference frames

Table 2: Origins of the local reference frames of each body segment. The numbers correspond to the black dots in **Figure 222** below.

Body Segment	Origin
Right Foot	Marker RHEE **(1)**
Left Foot	Marker LHEE **(2)**
Right Shank	Middle Point between markers RANK and RANKM **(3)**
Left Shank	Middle Point between markers LANK and LANKM **(4)**
Right Thigh	Middle Point between markers RKNE1 and RKNEM **(5)**
Left Thigh	Middle Point between markers LKNE1 and LKNEM **(6)**

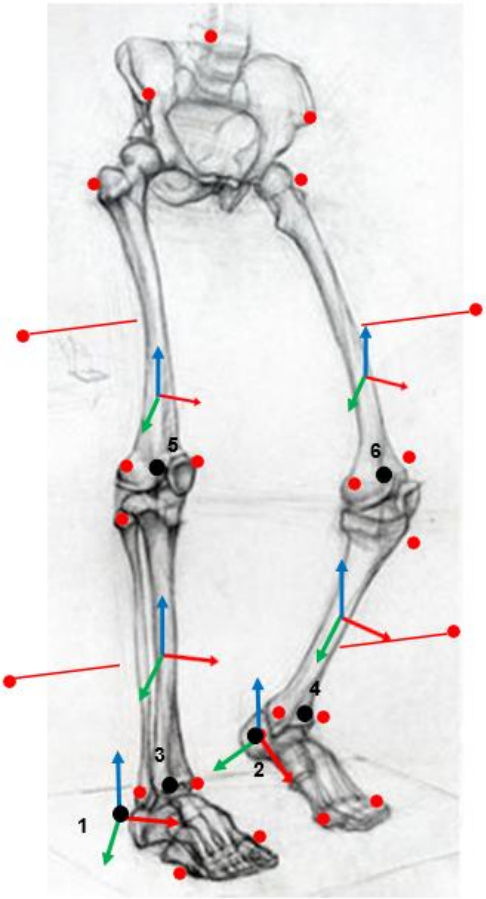

Figure 22: Representation of each referential. The x-axis, y-axis and z-axis are represented in red, blue and green, respectively. The black dots correspond to the origin of each referential.

Appendix B

B.1 Identification of the perturbations

B.1.1 Subject 1

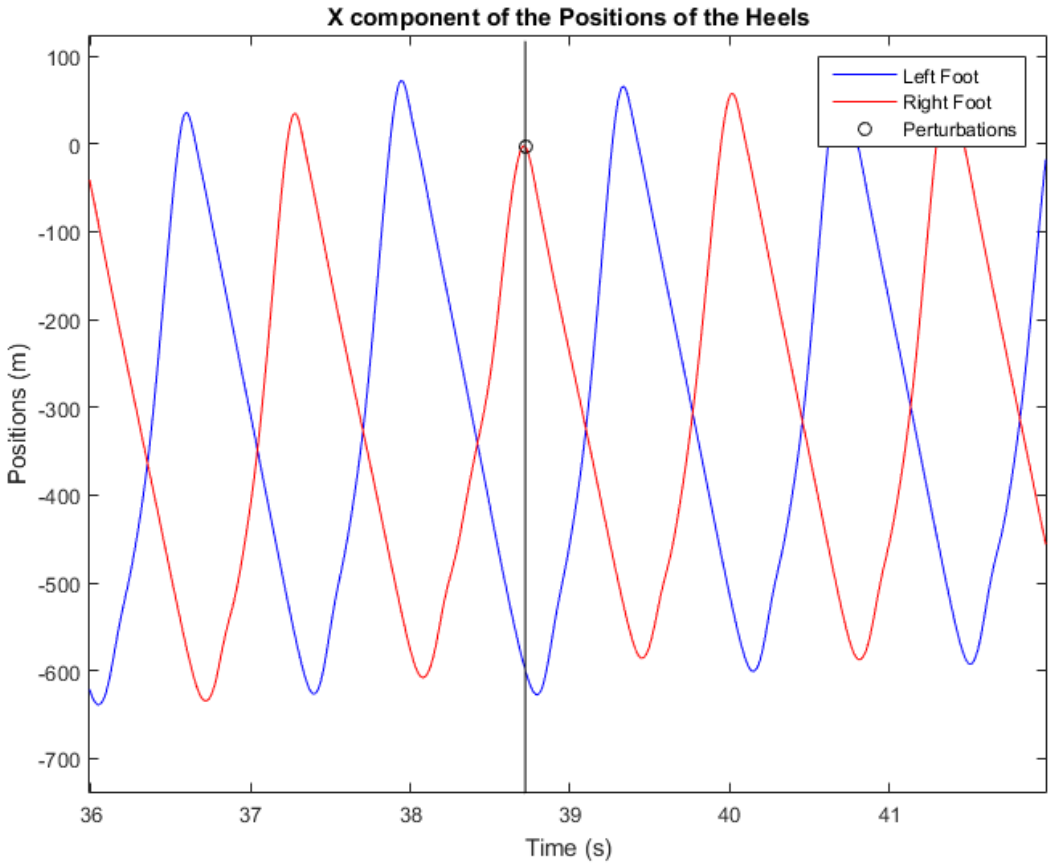

Figure 23: Identification of the perturbations by finding the lowest values of the right heel strikes, for subject 1.

B.1.2 Subject 2

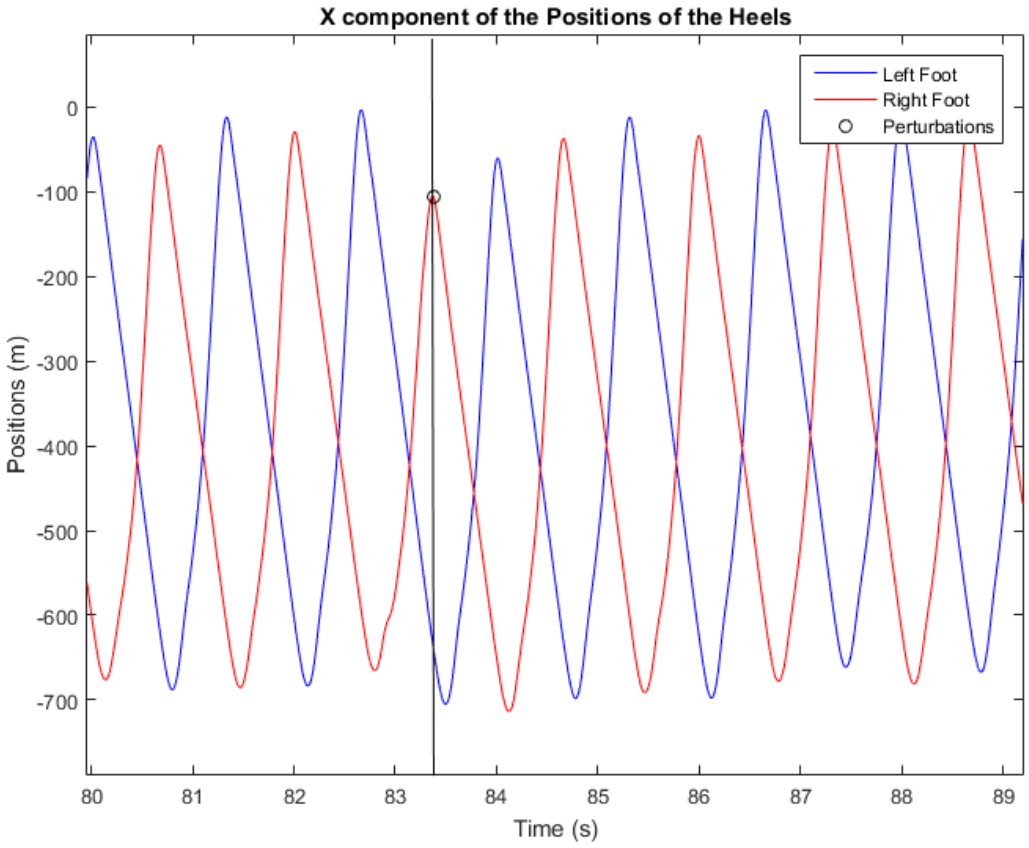

Figure 24: Identification of the perturbations by finding the lowest values of the right heel strikes, for subject 2.

Appendix C

C.1 Acceleration of the Shank

C.1.1 Subject 1

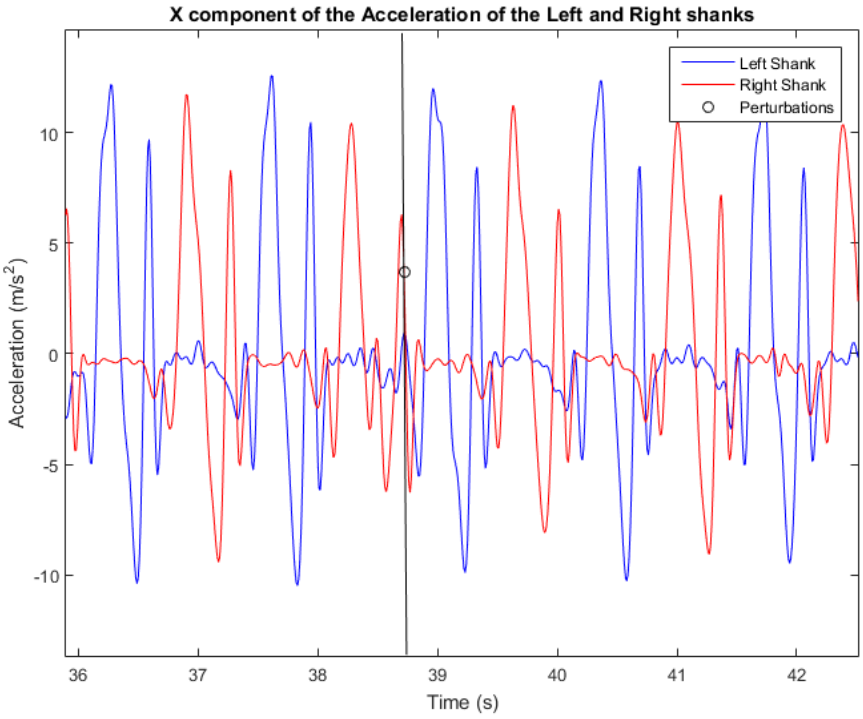

Figure 25: A region of interest of the X component of the acceleration $(m.s^{-2})$ of both left (blue) and right (red) shanks, in terms of time (s), for subject 1. The black points represent the perturbations.

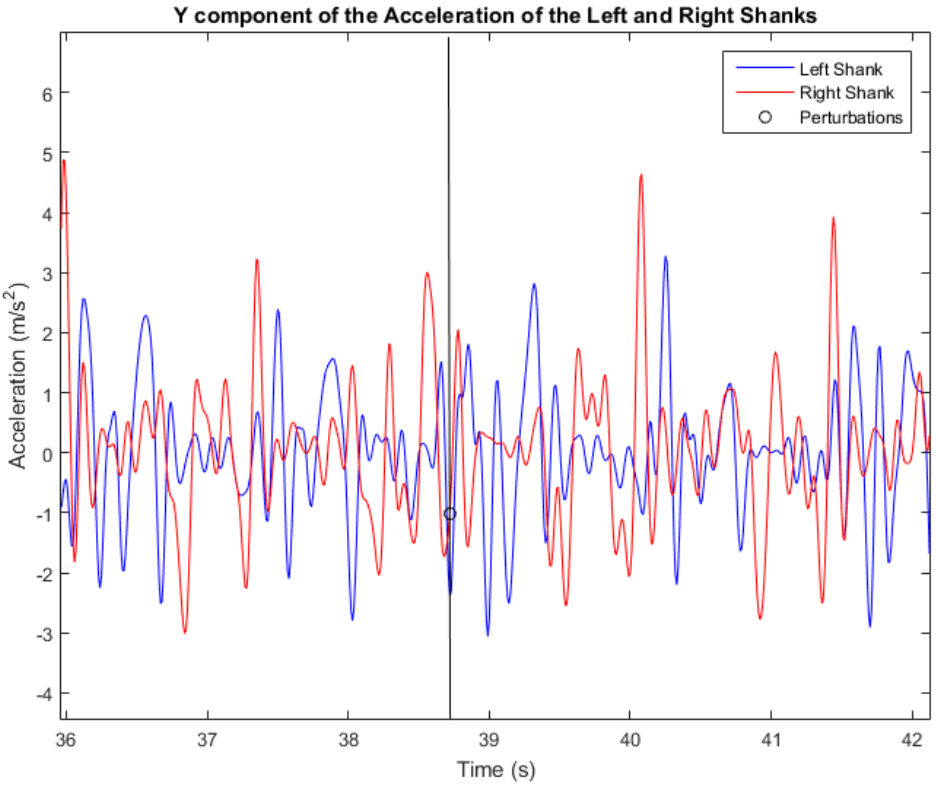

Figure 26: A region of interest of the Y component of the acceleration ($m.s^{-2}$) of both left (blue) and right (red) shanks, in terms of time (s), for subject 1. The black points represent the perturbations.

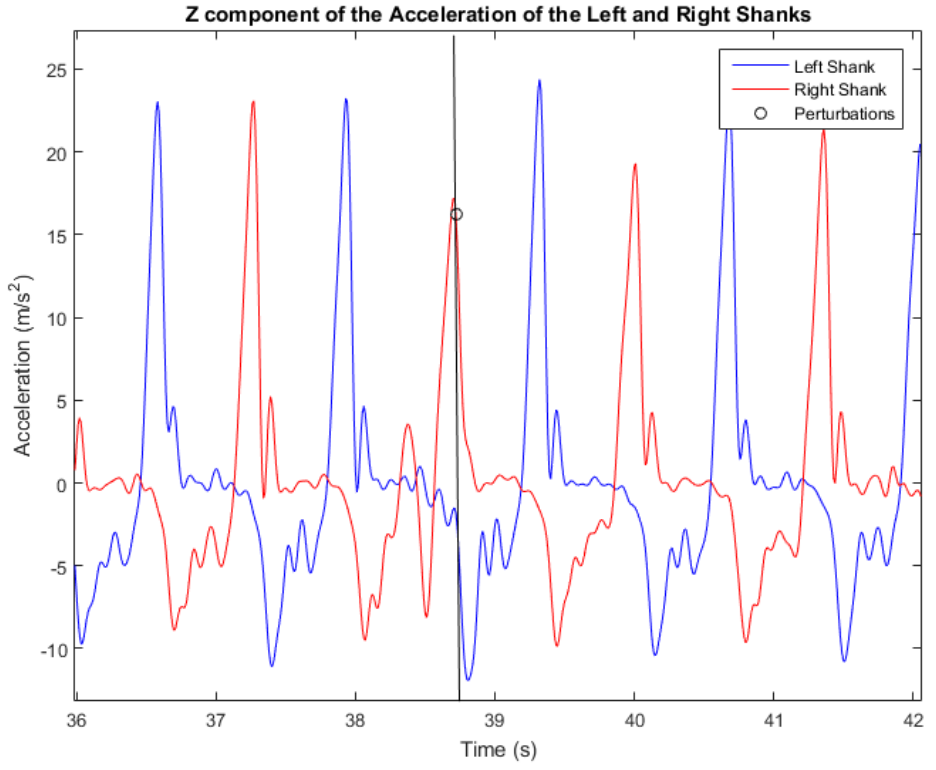

Figure 27: A region of interest of the Z component of the acceleration ($m.s^{-2}$) of both left (blue) and right (red) shanks, in terms of time (s), for subject 1. The black points represent the perturbations.

C.1.2 Subject 2

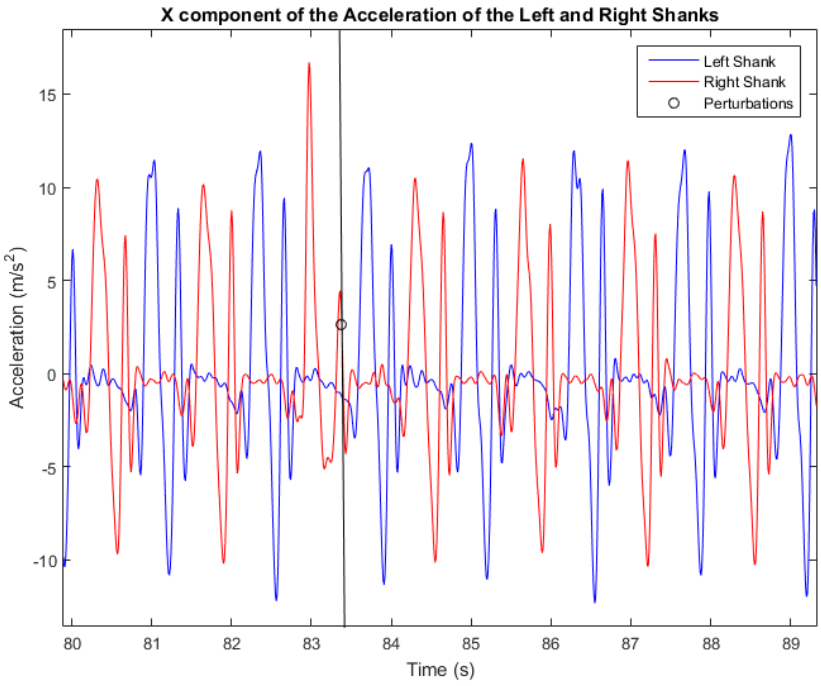

Figure 28: A region of interest of the X component of the acceleration ($m.s^{-2}$) of both left (blue) and right (red) shanks, in terms of time (s), for subject 2. The black points represent the perturbations.

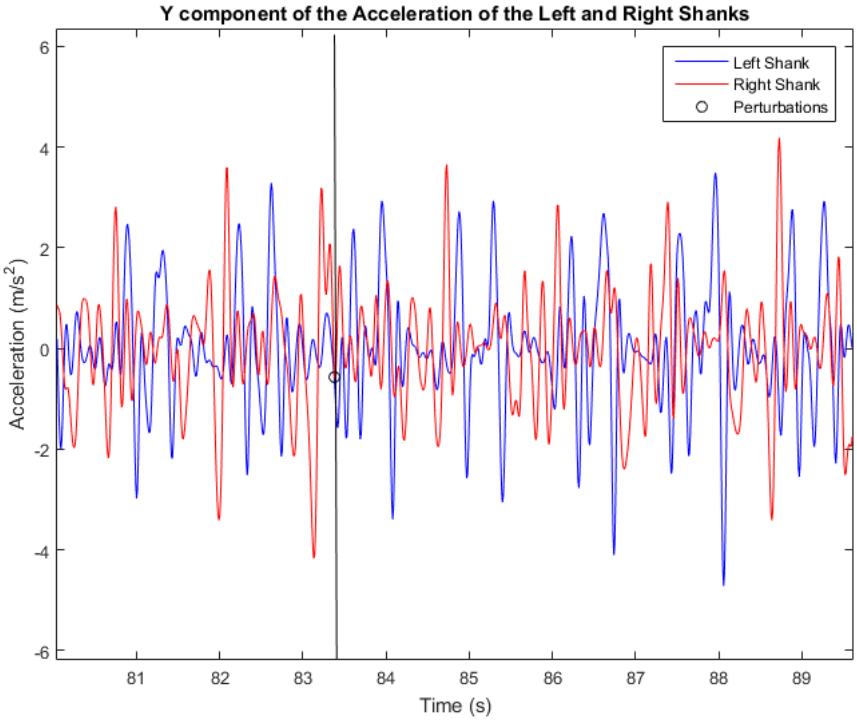

Figure 29: A region of interest of the Y component of the acceleration ($m.s^{-2}$) of both left (blue) and right (red) shanks, in terms of time (s), for subject 2. The black points represent the perturbations.

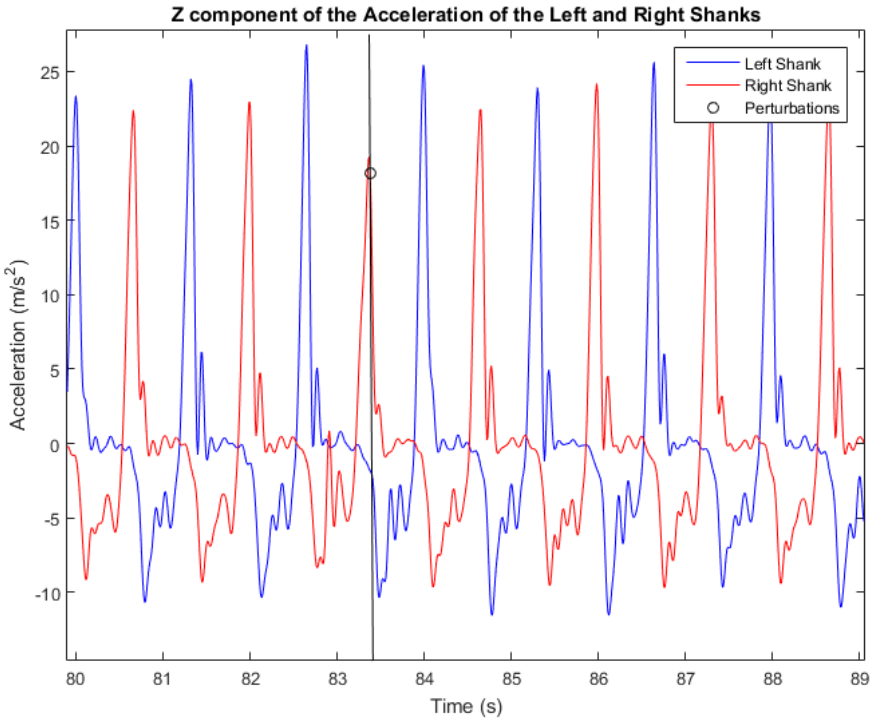

Figure 30: A region of interest of the Z component of the acceleration ($m.s^{-2}$) of both left (blue) and right (red) shanks, in terms of time (s), for subject 2. The black points represent the perturbations.

C.2 Acceleration of the Thigh

C.2.1 Subject 1

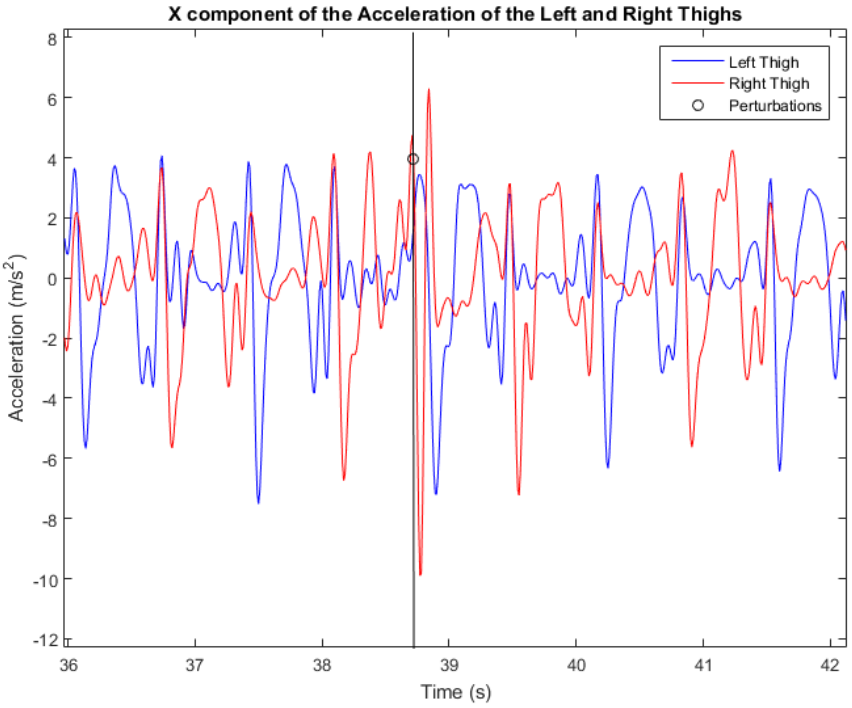

Figure 31: A region of interest of the X component of the acceleration ($m.s^{-2}$) of both left (blue) and right (red) thighs, in terms of time (s), for subject 1. The black points represent the perturbations.

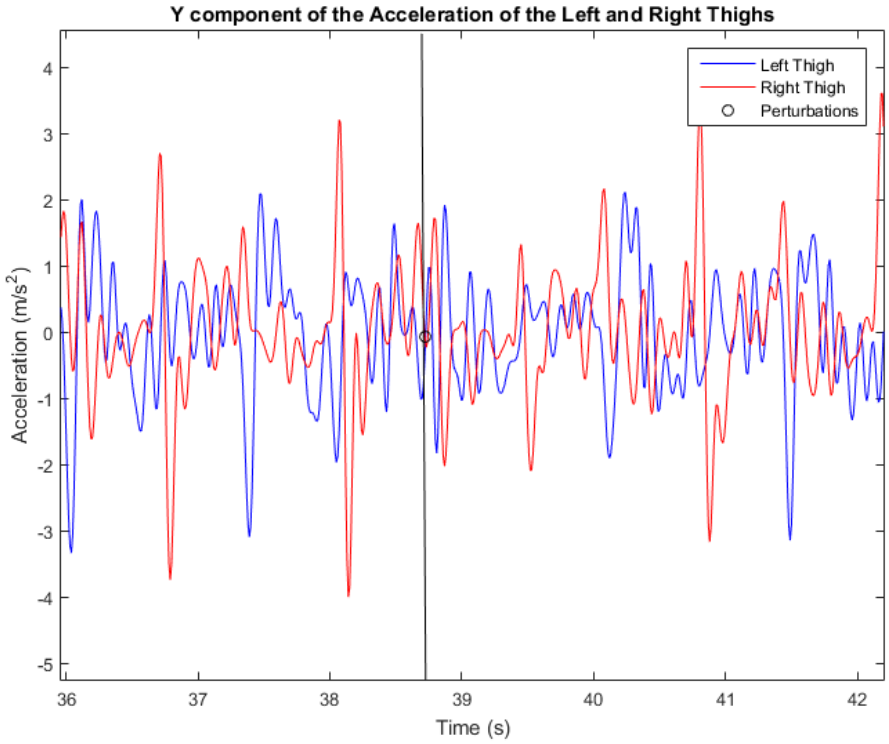

Figure 32: A region of interest of the Y component of the acceleration ($m.s^{-2}$) of both left (blue) and right (red) thighs, in terms of time (s), for subject 1. The black points represent the perturbations.

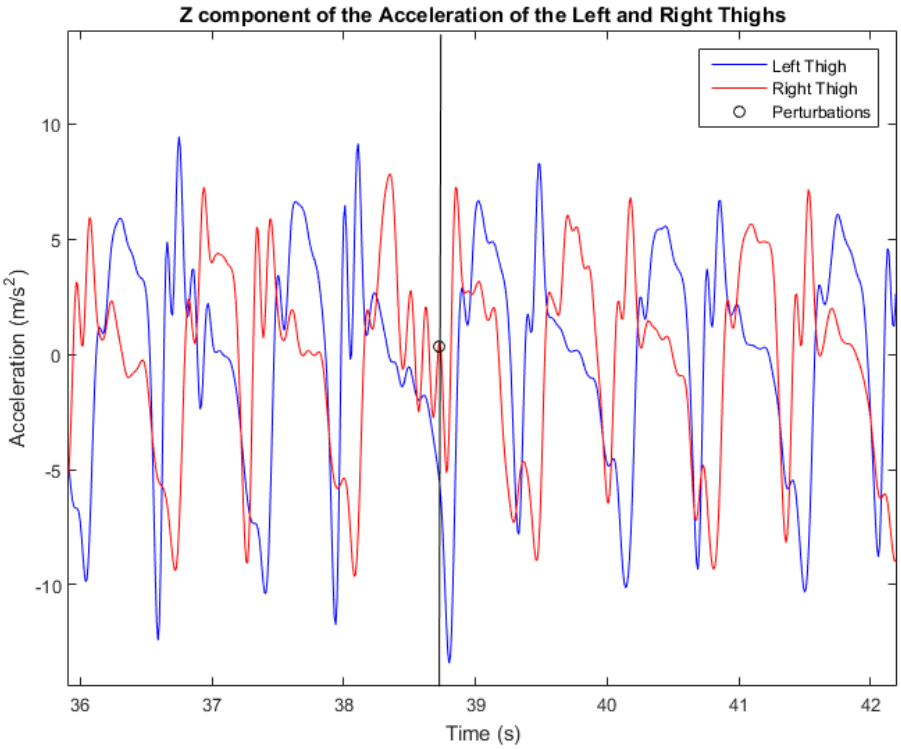

Figure 33: A region of interest of the Z component of the acceleration ($m.s^{-2}$) of both left (blue) and right (red) thighs, in terms of time (s), for subject 1. The black points represent the perturbations.

C.2.2 Subject 2

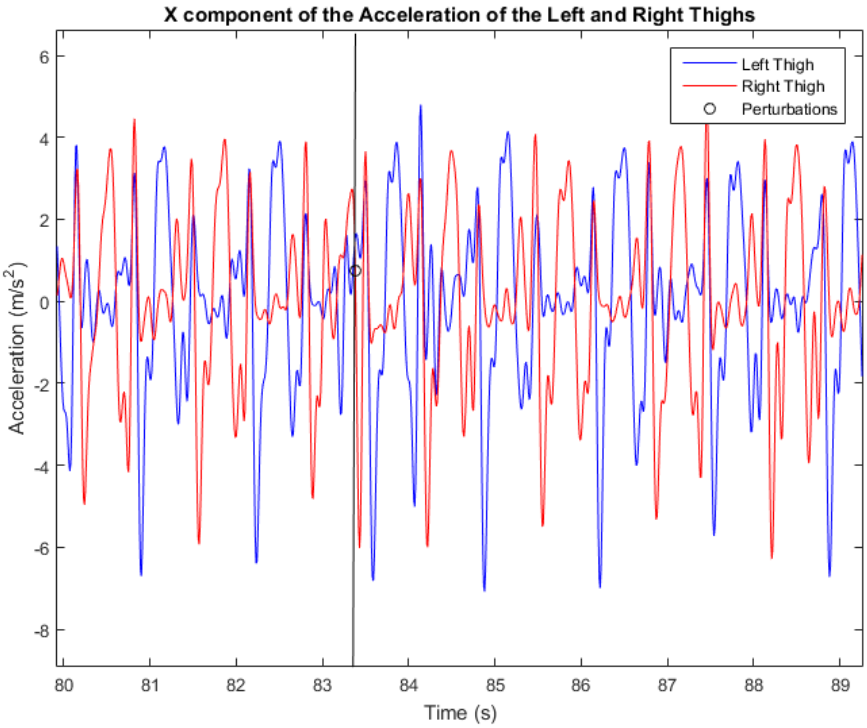

Figure 34: A region of interest of the X component of the acceleration ($m.s^{-2}$) of both left (blue) and right (red) thighs, in terms of time (s), for subject 2. The black points represent the perturbations.

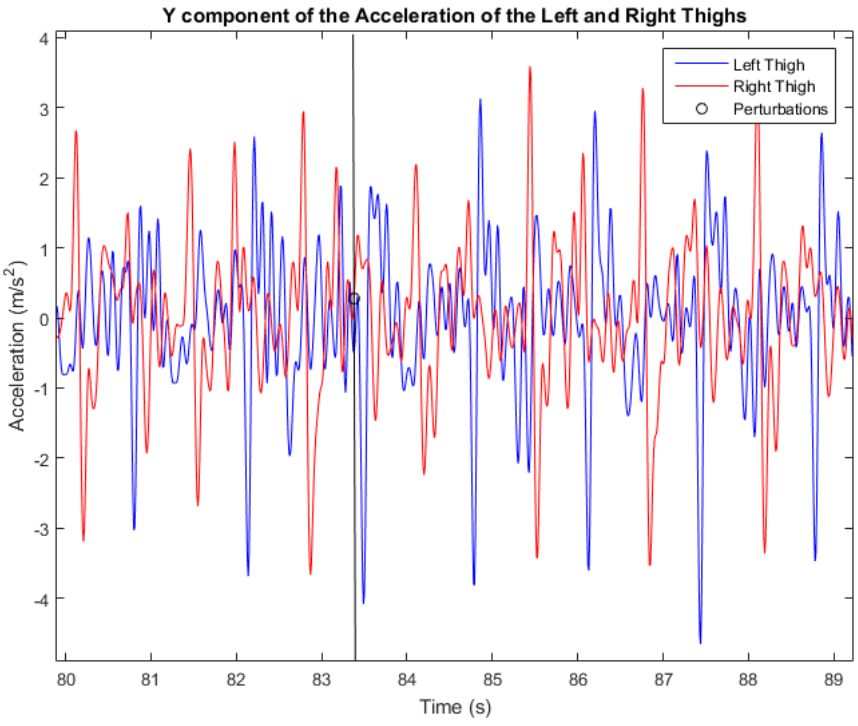

Figure 35: A region of interest of the Y component of the acceleration ($m.s^{-2}$) of both left (blue) and right (red) thighs, in terms of time (s), for subject 2. The black points represent the perturbations.

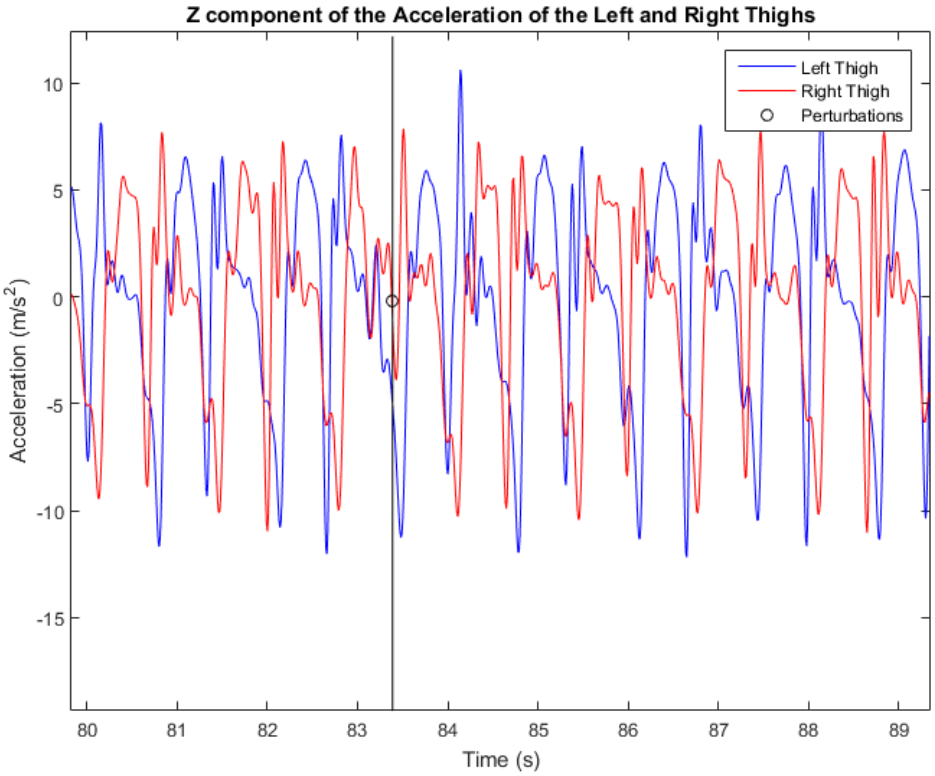

Figure 36: A region of interest of the Z component of the acceleration ($m.s^{-2}$) of both left (blue) and right (red) thighs, in terms of time (s), for subject 2. The black points represent the perturbations.

Appendix D

D.1 PCA signals obtained from several combinations

D.1.1 Subject 1

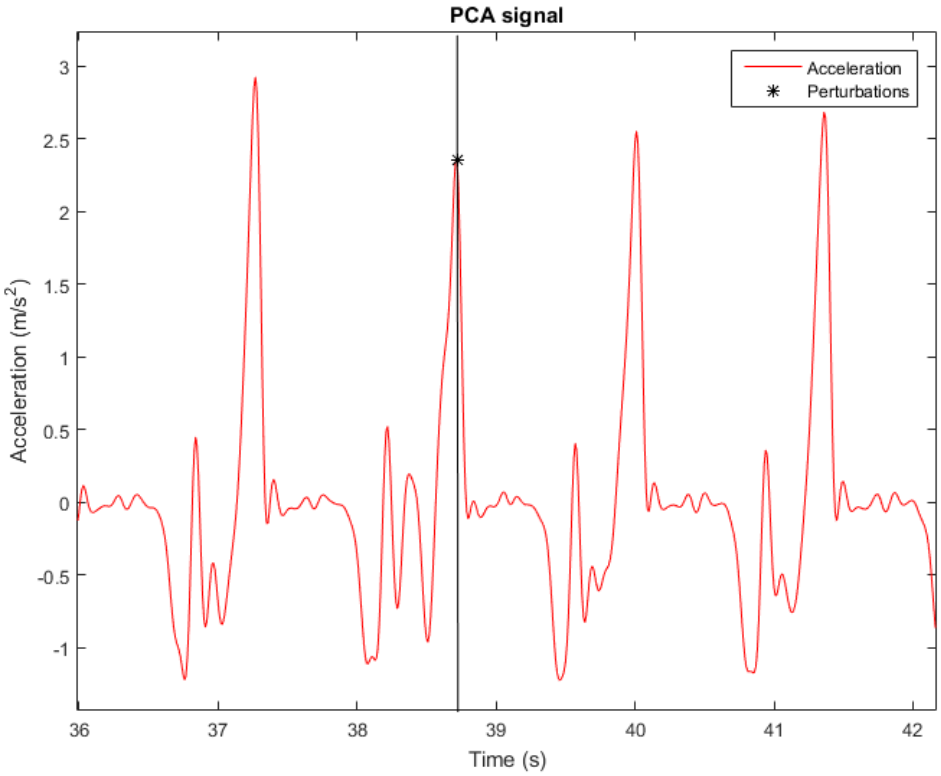

Figure 37: A region of interest of the signal obtained by applying the principal component analysis to the three components of the acceleration of the right foot, for subject 1. The perturbation is presented in black.

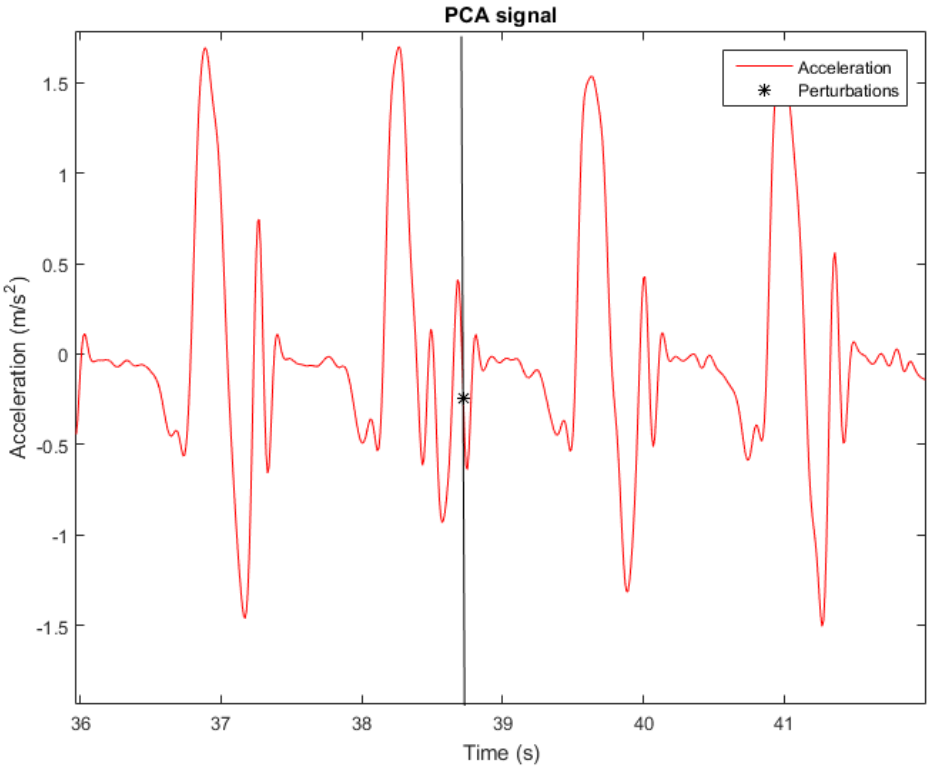

Figure 38: A region of interest of the signal obtained by applying the principal component analysis to the x component of the acceleration of the right foot, shank and thigh, for subject 1. The perturbation is presented in black.

D.1.2 Subject 2

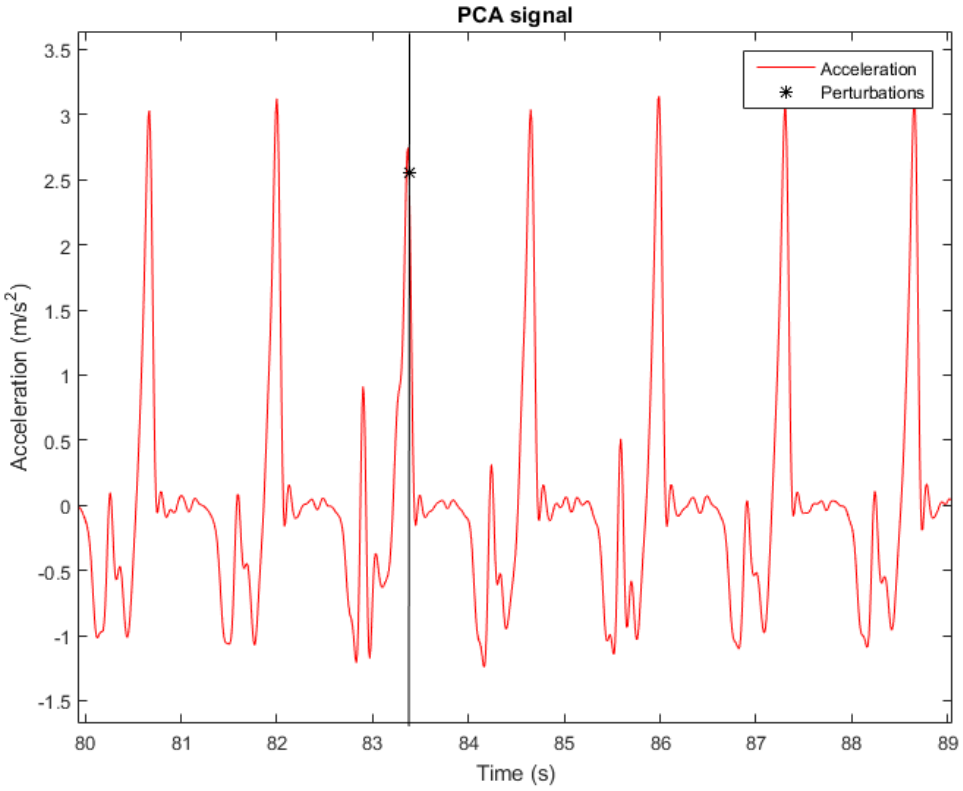

Figure 39: A region of interest of the signal obtained by applying the principal component analysis to the three components of the acceleration of the right foot, for subject 2. The perturbation is presented in black.

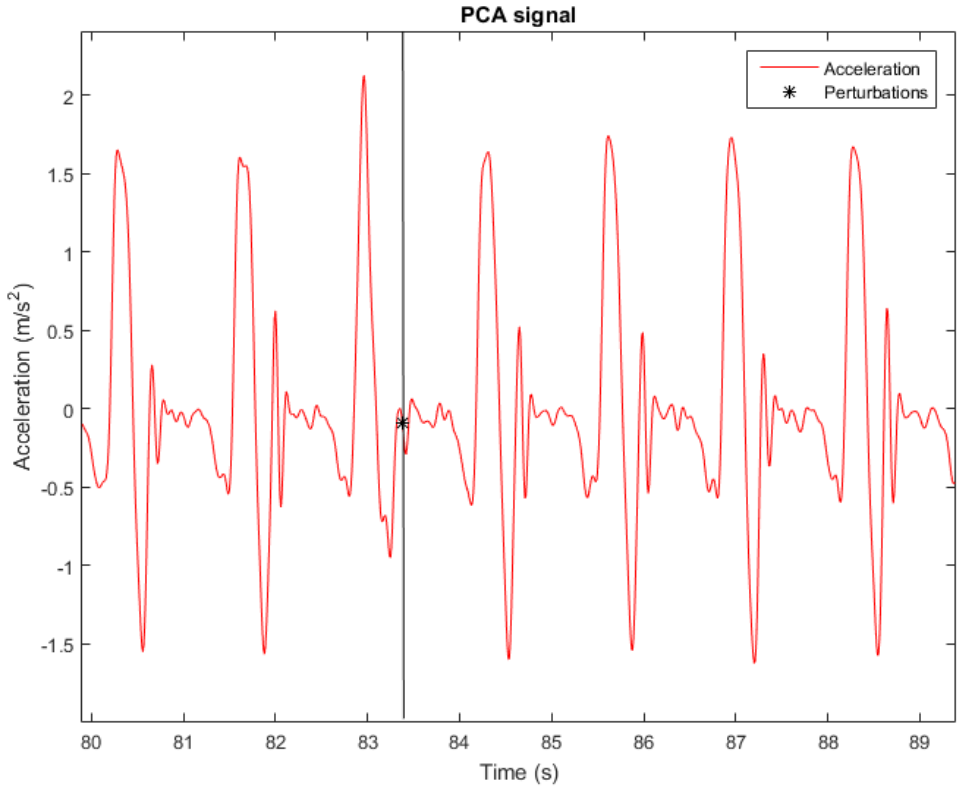

Figure 40: A region of interest of the signal obtained by applying the principal component analysis to the x component of the acceleration of the right foot, shank and thigh, for subject 2. The perturbation is presented in black.